© 2019 Nicklaus Richardson

OPTIMAL LIFT AND DRAG MODULATION HYPERSONIC CONTROL OPTIONS FOR HIGH BALLISTIC COEFFICIENT ENTRY VEHICLES AT MARS

BY

NICKLAUS O. RICHARDSON

THESIS

Submitted in partial fulfillment of the requirements
for the degree of Master of Science in Aerospace Engineering
in the Graduate College of the
University of Illinois at Urbana-Champaign, 2019

Urbana, Illinois

Adviser:

Assistant Professor Zachary R. Putnam

ABSTRACT

Future Mars entry, descent, and landing (EDL) missions will require larger mass vehicles and payloads, especially if humans are to land on the surface. Current Mars EDL technology relies heavily on Viking-era supersonic parachutes that are approaching their landed mass limits; however, supersonic retropropulsion (SRP) is a promising replacement for parachutes. Minimizing the propellant mass fraction (PMF) for SRP would enable larger payload masses. Maximizing the terminal descent initiation (TDI) altitude is also an important parameter for parachute deployment systems. The ability of different control methods, lift-only, drag-only, and both lift-and-drag control, to separately maximize TDI altitude and minimize PMF was assessed and compared over a range of entry conditions. Results show optimal control profiles that were always bang-bang with similar profiles for both cost functions. The number of switches that was optimal at a given entry state had a strong, direct relationship to entry flight-path angle with at most two-switches for lift control and at most four switches for drag control. Drag-only control was found to be better than lift-only control at steep entry flight path angles while lift-and-drag control was better than either at shallow entry flight-path angles. Adding drag control to lift-only systems was found to reduce PMF by approximately 40% across ballistic coefficients of 300 kg/m^2 to 600 kg/m^2 and entry velocities between 5 to 7 km/s. The set of feasible TDI states of each control method was assessed by linking the set of reachable TDI states from the hypersonic flight phase to the set of controllable TDI states from the propulsive descent phase. Increased controllability of lift-and-drag control and larger ballistic coefficients for drag control increases the size of the intersection of these two sets.

TABLE OF CONTENTS

NOMENCLATURE

A = Drag area, m^2

β_1 = Maximum vehicle ballistic coefficient, kg/m^2

β_2 = Minimum vehicle ballistic coefficient, kg/m^2

β_{ratio} = Vehicle ballistic coefficient ratio, n.d.

C_D = Coefficient of drag, n.d.

g = Instantaneous acceleration due to gravity at Mars, m/s^2

g_0 = Earth surface gravity, m/s^2

γ = Flight-path angle, rad

γ_0 = Entry flight-path angle, rad

γ_{goal} = Target terminal descent initiation flight-path angle, rad

H = Hamiltonian

h_{goal} = Target terminal descent initiation altitude, m

h = Altitude from planet surface, m

I_{sp} = Specific impulse, s

L/D = Vertical lift-to-drag ratio, n.d.

λ = Lagrange multiplier/costate

m = Vehicle mass, kg

R_p = Planet equatorial radius, m

ρ = Instantaneous atmospheric density, kg/m^3

σ = Bank angle, rad

S = Switching function

T = Thrust, N

t_0 = Initial time, s

t_f = Final time, s

u_D = Drag control variable, n.d.

u_L = Lift control variable, n.d.

u_T = Thrust control variable, n.d.

V = Planet relative velocity, m/s

V_{goal} = Target terminal descent initiation velocity, m/s

V_0 = Entry velocity, m/s

ΔV = Delta-v, m/s

$\boldsymbol{x}$ = State vector

CHAPTER 1: INTRODUCTION

Future Mars entry, descent, and landing (EDL) missions will require larger mass payloads. Current EDL systems are limited to Viking-era technology and are near landed mass limits [1]. Larger mass will directly increase ballistic coefficients as shown in the following equation:

$$\beta = \frac{m}{C_D A} \tag{1}$$

The ballistic coefficient can be seen as the ratio of inertial to aerodynamic forces. A large enough ballistic coefficient means the weight and momentum of the vehicle dominates the aerodynamic drag, and the vehicle cannot lose enough energy for parachute deployment to be feasible. Fig 1 shows different parachute deployment regimes, as shaded regions, within which parachute deployment is possible and lifting trajectories with a vertical lift-to-drag ratio of 0.18 for vehicles with varying ballistic coefficients. Subsonic and/or supersonic parachute deployment is possible for trajectories that pass through the shaded regions; however, larger ballistic coefficients, greater than approximately 150 kg/m^2, will not pass through any of these regions and will not be able to deploy a parachute using current technology. Developments must be made in parachute technology, parachute deployment altitude, or other descent methods if larger mass missions will be able to land on the Martian surface.

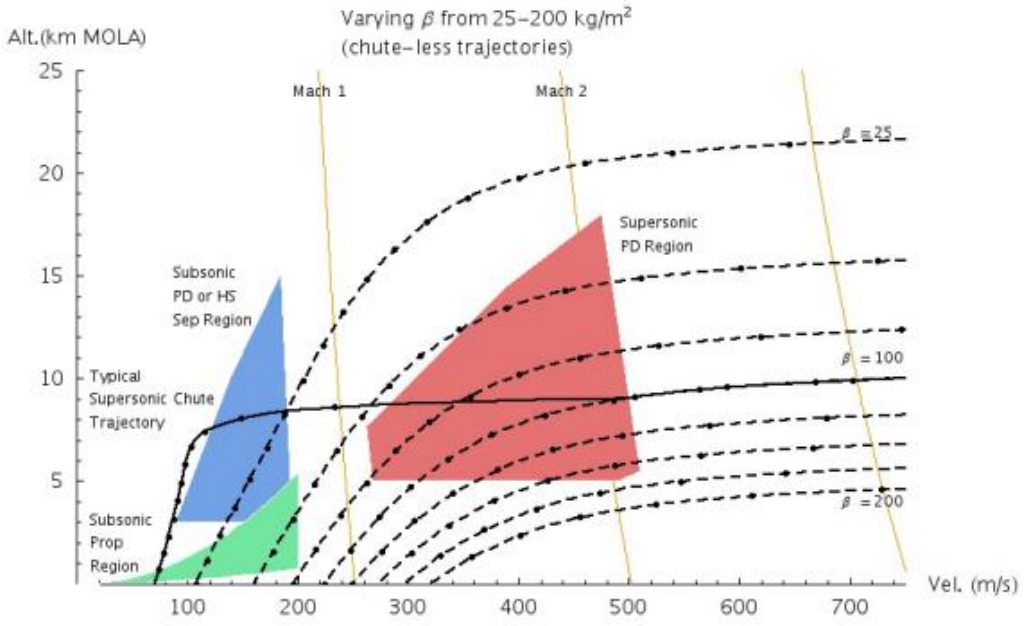

Fig 1. Deployment regimes for Viking-era parachutes over various ballistic coefficient trajectories [2]

One alternative descent method is supersonic retropropulsion. Supersonic retropropulsion (SRP) has been identified as a key technology for future development [1] as it can make up the difference in ΔV needed to land without relying on a parachute deployment. SRP technology requires significant advancement in current system-level components and modeling [3] and as such most recent SRP studies have focused on SRP system performance characterization and modeling [4-7]. Studies focusing on SRP have considered optimal ignition states but have not considered the hypersonic flight needed to reach these states. Prior hypersonic flight studies on the other hand have focused primarily on using the hypersonic control method, bank angle modulation, to maximize altitude at which descent is initiated as this maximization is beneficial to provide more time for parachute descent systems to decelerate [8-16]. Maximizing this altitude is not necessarily beneficial to SRP systems though. Propulsion systems benefit from minimization of the required

propellant necessary to sufficiently decrease the vehicle's velocity for landing; less mass dedicated to propellant led to more mass that can be allocated to payload, i.e. more landed mass. The propellant mass required for rocket propulsion is directly related to the required ΔV. The required ΔV is given by the rocket equation with gravity and drag losses with negligible off-axis thrust losses in the following equation [4]:

$$\begin{aligned} \Delta V_{\text{req}} &= \Delta V_{ideal} + \Delta V_{\text{gravity}} + \Delta V_{\text{gravity}} - \Delta V_{drag} + \Delta V_{thrust} \\ &= I_{sp} g_0 \ln\left(\frac{m_0}{m_0 - m_p}\right) + \int g \sin\gamma \, dt - \int \frac{D}{m} dt + 0 \end{aligned} \tag{2}$$

From Eq. (2), the minimum required propellant is achieved by minimizing the required change in velocity and gravity losses while maximizing drag deceleration. Maximization of the altitude that propulsive descent begins is generally not mass optimal as it does not grantee a minimum ΔV and may lead to significant gravity losses.

While most hypersonic control has focused on maximizing descent initiation attitude, a recent study by Lorenz and Putnam has explored the use of bank angle modulation to maximize the descent initiation for parachute descent systems and minimizing propellant mass fraction (PMF) for SRP systems [17]. While bank angle modulation represents the state-of-the-art in hypersonic reentry flight control, two other forms of flight control exist. The current study builds off the work done by Lorenz and Putnam, comparing other control methods ability to minimize the two cost functions. Since Lorenz and Putnam's work, few additional studies have been done. Notable are two studies done by Lu to modify Apollo powered descent guidance and develop propulsive descent initiation logic to incorporate near propellant-optimal initiation with

consideration to downrange error and robustness against dispersions [18] [19]. Lu's work does not focus on how the vehicle achieves the optimal descent initiation conditions though. The current study focuses on the ability of three different hypersonic control methods to achieve optimal terminal descent initiation states for parachute and SRP systems.

Prior to Mars Science Laboratory (MSL), all atmospheric flight through the Martian atmosphere was performed with no hypersonic flight control. MSL was the first Mars mission able to safely deliver its payload using a guided entry trajectory, minimizing range error while holding the majority of its lift up near the end of its flight to increase parachute deployment altitude [20]. This algorithm was divided into three phases. First, a prebank phase set initial vehicle bank angles and trim angle of attack. Then, the range control phase of this algorithm rotated the vehicle's lift vector about the velocity vector, bank angle control, to steer the vehicle to minimize downrange error and null cross range error based on a reference trajectory. Finally, a heading alignment where the vehicle is commanded to nearly full lift-up to maximize parachute deployment altitude. This lift modulation form of hypersonic control is based on an original algorithm from the Apollo missions, successfully being used to return all of the Apollo astronauts [21], and represents the state-of-the-art in entry vehicle control for both Earth and Mars entry.

Another control option is drag modulation through a jettison or deployment event of a drag skirt. By choosing a time to jettison or deploy an increased drag area, it can be shown that Mars EDL [22] or aerocapture at various planets can be achieved [23]. While this flight control option does not have the legacy of bank angle modulation, developments in deployable decelerators make it a good candidate for future use. As previously mentioned, one solution to landing larger mass payloads on Mars is to decrease the vehicle ballistic coefficient. Deployable decelerators accomplish this by increasing the drag area past limits due to launch vehicle fairing sizes which

lowers the ballistic coefficient as can be seen from Eq. (1). Because of this potential, decelerators have been identified by NASA as a key enabling technology for future investment [23] [24]. A system with a decelerator may be adapted to incorporate a jettison or deploy event for flight control. To maintain altitude, the drag modulation systems considered in this study all have nonzero L/D, but the lift is not used for steering.

The third form of hypersonic flight control is direct force control or a combination of lift and drag modulation. Direct force control uses modulation of the entry vehicle's angle-of-attack and side-slip angle to change the vehicle's trim conditions and vary both the lift and drag vector direction and magnitude. There are two methods to accomplish this. The first is through aerodynamic trim tabs [26] [27]. Trim tabs are aerodynamic control surfaces that can be set to varying cant angles to trim an entry vehicle to a non-zero angle of attack and side-slip angle without the need for a center of mass offset. The second method is moving mass actuation. By moving an internal mas, a center of mass offset to can be created to create a trim condition, varying vehicle lift magnitude and direction with limited drag control but does not directly interact with the hypersonic flow. Moving mass actuation has been studied as a replacement for bank angle modulation-based guidance [28] [29]. Direct force control can be thought of as a combination of lift and drag modulation; however, another method to control both lift and drag may be bank angle control of a drag skirt vehicle that incorporates a jettison or deployment event. This combination would increase system complexity than individual lift or drag control however.

The current work builds on work done by Lorenz and Putnam [17]. Terminal descent initiation (TDI) altitude maximization and PMF minimization are explored through an optimal control problem formulation with a comparison of lift-only control, drag-only control, and both lift-and-drag control's ability to maximize or minimize these two cost functions. Minimization of

the PMF is performed through a two-phase optimal control problem with an initial hypersonic flight phase followed by a propulsive descent phase. The two-phase problem is constrained to enter the Martian atmosphere at a specified entry state and end at a specified landing state, creating a set of reachable TDI states through hypersonic flight control and a set of controllable TDI states through thrust control during propulsive descent. The ability of each method to target the controllable set of TDI states is also compared.

CHAPTER 2: METHODOLOGY

2.1 Vehicle, Flight, and Environmental Parameters

Vehicle and flight parameters were chosen to be similar to Lorenz and Putnam [17]. The range of vehicle parameters are shown in Table 1. When not specified, all parameters are taken to be nominal values. The nominal lift-to-drag ratio was selected to be similar to the lift-to-drag ratio of MSL [20]. The ratio of ballistic coefficients for drag modulation was selected to focus around moderate increases in vehicle radius with an upper limit to include large-area-increase drag skirt systems such as the Adaptive Deployable Entry and Placement Technology (ADEPT) [30].

Table 1 Vehicle Parameters

Parameter	Lower Bound	Nominal	Upper Bound
Lift-to-Drag Ratio, n.d.	0	0.24	0.30
Ballistic Coefficient, kg/m^2	300	450	600
Ballistic Coefficient Ratio, n.d.	1	2	20
Initial Mass, kg	--	602	--
Specific Impulse, s	--	300	--
Thrust-to-Weight Ratio, n.d.	--	4	--

The range of entry trajectory parameters are shown in Table 2. Nominal entry conditions were based off of MSL entry interface conditions [20]. The initial planet-relative velocity of the vehicle and initial flight-path angle were varied to span possible entry conditions of the spacecraft based on Earth-Mars trajectories with a transfer time of more than 220 days [31]. The range of entry flight-path angles incorporates all previous U.S. Mars missions [1]. The TDI velocity range was chosen to expand on the range selected by Lorenz [17] with a lower limit to show more reachable states for large ballistic coefficient ratio drag-only control systems.

Table 2 Flight Parameters

Parameter	Lower Bound	Nominal	Upper Bound
Entry Velocity, m/s	5000	5850	7000
Entry Flight-Path Angle, deg.	-25.0	-15.5	-7.0
Entry Altitude, km	--	125	--
TDI Velocity, m/s	150	480	950
Reference Density, kg/m^3	--	0.02	--
Reference Altitude, km	--	0	--
Scale Height, km	--	11.1	--

A higher-fidelity model using bank-angle acceleration control and the Mars Global Reference Atmospheric Model (Mars-GRAM) was previously shown to yield similar results with the main structure of solutions preserved in lower fidelity modelling [17]; therefore, the Martian environment was modelled using an exponential atmosphere and inverse-square gravity to reduce computation time.

2.2 Hypersonic Flight Dynamics

The vehicle dynamics during hypersonic flight were modeled using the two-dimensional equations of motion for atmospheric flight, assuming a non-rotating planet, modified with control variables, u_L and u_D, as follows:

$$\dot{V} = -\frac{\rho V^2}{2\beta_1} u_D - g \sin\gamma \tag{3}$$

$$\dot{\gamma} = \frac{\rho V}{2\beta_1}\left(\frac{L}{D}\right) u_L u_D - \frac{g}{V}\cos\gamma + \frac{V\cos\gamma}{R_p + h} \tag{4}$$

$$\dot{h} = V \sin\gamma \tag{5}$$

Continuum flow and constant aerodynamic coefficients were assumed. Lift control was modeled using the control variable, $u_L \in [-1,1]$, which can be described by bank angle control with the following equation:

$$u_L = \cos\sigma \tag{6}$$

Bank angle control is accomplished by rotating the lift vector, created by a center-of-mass offset, angle of attack, or asymmetry in the aeroshell, around the vehicle's velocity vector to control the direction of the lift. This control of the lift vector direction changes the magnitude of the vertical lift-to-drag ratio by trading lift in the vertical direction with lift in the cross-range direction. Typically, a limit on the bank angle is placed to allow for sufficient control in both directions. All hypersonic flight control using only lift modulation is referred to as lift-only control.

Drag control is performed by modifying the vehicle ballistic coefficient, assuming a constant lift-to-drag ratio, using the control variable, $u_D \in [1, \beta_{ratio}]$, where β_{ratio} is the ratio of maximum to minimum ballistic coefficients for a drag modulation system given by:

$$\beta_{ratio} = \frac{\beta_1}{\beta_2} \geq 1 \tag{7}$$

The ballistic coefficient ratio is defined as always greater than one as β_1 represents the maximum ballistic coefficient. Drag modulation can be accomplished by the jettison/retraction or deployment of additional area exposed to the flow to decrease or increase, respectively, an entry vehicle's drag area, controlling the vehicle's rate of energy dissipation. The maximum ballistic

coefficient can be thought of as a retracted or jettisoned drag skirt vehicle configuration while the minimum ballistic coefficient can be thought of as a drag skirt deployed configuration. All hypersonic flight control using only drag modulation is referred to as drag-only control, even if L/D is nonzero.

Hypersonic flight control using both lift and drag modulation is referred to as lift-and-drag control. The inclusion of both lift and drag control may be thought of as two possible configurations. First is a combination of bank angle control and drag modulation. A lifting entry vehicle with a drag skirt able to control its bank angle may be also be able to incorporate a drag-skirt jettison or deployment event, accomplishing both lift and drag modulation. Another possibility is direct force control through either trim tabs or moving-mass actuation. The lift-and-drag control system is modeled such that control of the lift-to-drag ratio and ballistic coefficient are independent. In reality, modifying the total angle of attack to change L/D or C_L will also result in a change in C_D.

2.3 Propulsive Descent Dynamics

Immediately after the hypersonic flight, the vehicle initiates powered flight described by the following two-dimensional entry equations:

$$\dot{V} = -g \sin\gamma - g\left(\frac{T}{W}\right)u_T \tag{8}$$

$$\dot{\gamma} = -\frac{g}{V}\cos\gamma + \frac{V\cos\gamma}{R_p + h} \tag{9}$$

$$\dot{h} = V \sin\gamma \tag{10}$$

$$\dot{m} = -\frac{mg}{I_{sp}g_0}\left(\frac{T}{W}\right)u_T \tag{11}$$

Eqs. (8)-(11) assume the use of a gravity turn maneuver, thrust in the opposite direction of velocity, and negligible aerodynamic forces relative to thrust. A gravity turn maneuver is not propellant optimal [7] but is a common method to model propulsive descent in many studies [4] [33-35]. Neglecting drag is generally a conservative assumption for propulsive descent and is more accurate for high ballistic coefficient vehicles [4]. Again, an inverse-square gravity model was used.

2.4 Optimal Control Problem Formulation

The ability of the three control methods to minimize two different objective functions was assessed. The first objective function is the maximization of the terminal descent initiation (TDI) altitude while the second objective function is to minimize the propellant required by the propulsive descent system.

Because the control is linear with respect to the dynamics for the lift-only and drag-only cases, the optimal control will be bang-bang by Pontryagin's Minimum Principle. Pontryagin's Minimum Principle states that the optimal control must minimize the Hamiltonian and is given as follows:

$$H(\boldsymbol{\lambda}^*, \boldsymbol{x}^*, \boldsymbol{u}^*, t) \leq H(\boldsymbol{\lambda}^*, \boldsymbol{x}^*, \boldsymbol{u}, t) \quad (12)$$

The Hamiltonian is defined as follows:

$$H = L(\boldsymbol{x}, \boldsymbol{u}, t) + \boldsymbol{\lambda}^{\boldsymbol{T}}(t)\boldsymbol{f}(\boldsymbol{x}, \boldsymbol{u}, t) \quad (13)$$

where L is the integrand of the Lagrange form cost function, the Lagrangian, and $\boldsymbol{f}$ is a vector of constraints, such as system dynamics. If the control is linear with respect to the cost and the dynamics, the optimal control to minimize the Hamiltonian must be at one of the bounds of the control, bang-bang. A bang-bang controller switches the control based off the sign of a switching function, defined as the negative change in the Hamiltonian due to a control input. When the switching function is positive, the control decreases the Hamiltonian, so a maximum control value is optimal to minimize the Hamiltonian. When the switching function is negative, the applied control increases the Hamiltonian, so a maximum control value minimizes the Hamiltonian. The switching function is computed as follows:

$$S = -\frac{\partial H}{\partial \boldsymbol{u}} \tag{14}$$

where **u** is a vector of controls.

2.4.1 TDI Altitude Maximization

Maximizing TDI altitude is typically associated with parachute-based terminal descent systems; a higher TDI (parachute deploy) altitude improves the total deceleration impulse provided by the parachute by increasing the time available for descent. The optimal control problem to maximize TDI altitude is given with a Mayer form cost function as follows:

$$\begin{gathered} max\ h(t_f) \\ \text{s.t. } \boldsymbol{f}(\boldsymbol{x}, \boldsymbol{u}, t) = \dot{\boldsymbol{x}}(\boldsymbol{x}, \boldsymbol{u}) \\ V(t_f) = 480\ m/s \end{gathered} \tag{15}$$

The initial state of the optimal control problem is specified with various entry conditions. While the optimal control problem was implemented in Mayer cost form, to compute the Hamiltonian and apply Pontryagin's Minimum Principle, the cost was converted to Lagrange cost form. The Lagrange cost is given by the following:

$$J = -\int_{t_0}^{t_f} \dot{h}\, dt = -\int_{t_0}^{t_f} V \sin\gamma\, dt \tag{16}$$

Because Lagrangian does not depend on the control, by Pontryagin's Minimum Principle, the optimal control to minimize the Hamiltonian will be bang-bang if the control is also linear with respect to the dynamics.

The ability of three different hypersonic trajectory control strategies to maximize TDI altitude at the end of the hypersonic flight phase was assessed using the General Pseudospectral Optimization Software (GPOPS) package [32]. While the TDI state was constrained to have a final velocity of 480 m/s, GPOPS requires bounds on other the final state variables and final time. The final flight-path angle was constraint to be between -90º and 90º. The final altitude was constrained between -100 km and 100 km to improve solution convergence. Heuristic constraints on the final time were used to further improve convergence depending on the control method and how close the initial conditions were to yielding a skip-out trajectory as an arbitrarily large guess on final time often resulted in a non-converged solution for trajectories with a small time-of-flight.

For lift-only trajectory control, the final time was constrained to be at most 750 s. A single final time constraint was used for lift-only trajectory control over all initial states examined as there were no convergence issues associated with this single constraint. For drag-only trajectory

control, the final time was constrained to be at most 750 s expect at initial flight-path angles greater than -15.1° where the time-of-flight began to gradually increase beyond 750 s due to large lofting near the skip-out boundary. Above an initial flight-path angle of -15.1°, final time was constrained to be at most arbitrarily large at 15,000 s. Lift-and-drag control systems were found to be more sensitive to final time constraints than either lift-only or drag-only control; therefore, an arbitrarily large time, such as 15,000 s, was not able to be used without convergence issues. Lift-and-drag control final time was constrained to be at most 400 s expect near skip-out where it was constrained to be at most 750 s. Similar to the drag-only case, near skip-out was defined as any initial flight-path angle above -9.5° or at initial flight-path angles of -10.1° when the initial velocity was above 5.9 km/s.

2.4.1.1 Lift-only Optimal Control

Lift-only control dynamics were modeled as described in Section 2.2 with the drag control variable, u_D, set to a value of 1, maximum ballistic coefficient. The resulting TDI altitude maximization optimal control problem's Hamiltonian is as follows:

$$H = -V\sin\gamma + \lambda_V\left(-\frac{\rho V^2}{2\beta_1} - g\sin\gamma\right) + \lambda_\gamma\left(\frac{\rho V}{2\beta_1}\left(\frac{L}{D}\right)u_L - \frac{g}{V}\cos\gamma + \frac{V\cos\gamma}{R_p + h}\right) + \lambda_h(V\sin\gamma) \qquad (17)$$

Because the Hamiltonian is linear with respect to the control, the optimal control will be bang-bang. The optimal control will minimize the Hamiltonian at one of the bounds based on the sign of the following switching function:

$$S = -\lambda_\gamma \frac{\rho V}{2\beta_1}\left(\frac{L}{D}\right) \tag{18}$$

Because the atmospheric density, velocity, ballistic coefficient, and lift-to-drag ratio are strictly positive, the sign of Eq. (18) is dependent only on the flight-path angle costate; the optimal control will be at its upper bound when the flight-path angle costate is negative or at its lower bound when the costate is positive.

2.4.1.2 Drag-only Optimal Control

Drag-only control dynamics were modeled as described in Section 2.2 with the lift control variable, u_L set to a value of 1, or lift-up. The Hamiltonian of the optimal control problem is as follows:

$$H = -V sin\gamma + \lambda_V\left(-\frac{\rho V^2}{2\beta_1}u_D - g\sin\gamma\right) + \lambda_\gamma\left(\frac{\rho V}{2\beta_1}\left(\frac{L}{D}\right)u_D - \frac{g}{V}\cos\gamma + \frac{V\cos\gamma}{R_p + h}\right) + \lambda_h(V\sin\gamma) \tag{19}$$

The drag-only control with respect to the Hamiltonian is linear; the optimal control will again be bang-bang. The switching function for this case is as follows:

$$S = -\left(\lambda_\gamma \frac{\rho V}{2\beta_1}\left(\frac{L}{D}\right) - \lambda_V \frac{\rho V^2}{2\beta_1}\right) \tag{20}$$

2.4.1.3 Lift-and-drag Optimal Control

Lift-and-drag control dynamics are modeled as described in Section 2.2 with both control variables included. The Hamiltonian of the optimal control problem is as follows:

$$H = -Vsin\gamma + \lambda_V\left(-\frac{\rho V^2}{2\beta_1}u_D - g\sin\gamma\right) + \lambda_\gamma\left(\frac{\rho V}{2\beta_1}\left(\frac{L}{D}\right)u_L u_D - \frac{g}{V}\cos\gamma + \frac{V\cos\gamma}{R_p + h}\right) + \lambda_h(V\sin\gamma) \quad (21)$$

The lift-and-drag control optimal control problem's Hamiltonian differs from the individual control problems' Hamiltonians due to the non-linearity of the control variables in the derivative of the flight-path angle; however, the optimal control is still bang-bang. The lift and drag control that minimizes the Hamiltonian is still at its bounds as the two control variables are separately linear with respect to the Hamiltonian, and the lift control is independent of the drag control. The switching function for the lift control portion of the lift-and-drag system is as follows:

$$S_L = -\lambda_\gamma \frac{\rho V}{2\beta_1}\left(\frac{L}{D}\right)u_D \quad (22)$$

While the switching function is a function of the drag control, the drag control is strictly positive; the sign of the switching function and optimal lift control are dependent only on the sign of the flight-path angle costate and independent of the drag control. The control to minimize the Hamiltonian will be at the bounds for both lift and drag control as a result of this independence.

The switching function of the drag control portion of the lift-and-drag system is given as follows:

$$S_D = -\left(\lambda_\gamma \frac{\rho V}{2\beta_1}\left(\frac{L}{D}\right)u_L - \lambda_V \frac{\rho V^2}{2\beta_1}\right) \quad (23)$$

Because the lift control variable is either -1 or +1, the optimal drag control will be dependent on the lift control; however, the lift control is not dependent on the drag control and the lift control variable can be seen as an independent variable in the drag control switching function, similar to the two costates.

2.4.2 Propellant Mass Fraction Optimal Propulsive Descent

While the maximization of TDI altitude is important for parachute descent systems, larger mass missions will likely not be able to use parachutes. SRP is a likely candidate for these larger mass missions. For SRP descent systems, a more important parameter to minimize is the required propellant, expressed through the propellant mass fraction (PMF). Minimizing the PMF allows for a more mass for the payload, other subsystems, or reduced total vehicle mass.

To minimize the PMF, a two-stage optimal control problem was formulated with an initial hypersonic flight phase, using one of the three hypersonic control methods, and a final propulsive descent phase using a gravity turn as described in Section 2.3. The two-phase optimal control problem to minimize the PMF is as follows:

$$\begin{aligned} &\text{minimize } PMF \\ &\text{s.t. } f(\boldsymbol{x}, \boldsymbol{u}) = \begin{cases} \dot{\boldsymbol{x}}_{\boldsymbol{hyp}}, & for\ t \leq t_{TDI} \\ \dot{\boldsymbol{x}}_{\boldsymbol{SRP}}, & else \end{cases} \\ &\boldsymbol{x}(t_{f,1}) = \boldsymbol{x}(t_{0,2}) \\ &t_{f,1} = t_{0,2} \end{aligned} \tag{24}$$

where the PMF is given by the following:

$$PMF = 1 - \frac{m(t_{f,2})}{m(t_{0,2})} \tag{25}$$

The initial mass of the propulsive descent phase is constant; therefore, the PMF depends only on the final mass, or propellant used, during descent. The dynamics switch from hypersonic flight to propulsive descent at TDI as described in Sections 2.2 and 2.3, respectively. At TDI, the final state and time of the hypersonic flight phase must be the same as the initial state and time of the propulsive descent phase. The boundary conditions of this problem are to enter the atmosphere at an initial altitude of 125 km, initial atmosphere-relative velocity of 5845 m/s, and initial flight-path angle of -15.5º and land with a terminal velocity of 1 m/s and terminal altitude of 0 m for the propulsive descent phase. A constant thrust-to-weight ratio of 4 was used, referenced to the surface gravity of Mars.

2.4.2.1 Optimal Control Profiles for PMF Minimization

The Hamiltonian of the two-phase optimal control problem is discontinuous due to the piece-wise dynamics. The Lagrangian term of the Hamiltonian is as follows:

$$L = -\dot{m} = \begin{cases} 0, & for\ t < t_{TDI} \\ \dfrac{mg}{g_0 I_{sp}}\left(\dfrac{T}{W}\right)u_T, & else \end{cases} \tag{26}$$

The Hamiltonian for the lift-and-drag hypersonic control and the propulsive descent thrust control phase, respectively, are given in the following equations:

$$H_1 = \lambda_V \left(-\frac{\rho V^2}{2\beta_1} u_D - g \sin\gamma \right) + \lambda_\gamma \left(\frac{\rho V}{2\beta_1} \left(\frac{L}{D} \right) u_L u_D - \frac{g}{V} \cos\gamma + \frac{V \cos\gamma}{R_p + h} \right) + \lambda_h (V \sin\gamma) \quad (27)$$

$$H_2 = \frac{T u_T}{g_0 I_{sp}} + \lambda_V \left(-g \sin\gamma - \frac{T u_T}{m} \right) + \lambda_\gamma \left(-\frac{g}{V} \cos\gamma + \frac{V \cos\gamma}{R_p + h} \right) + \lambda_h (V \sin\gamma) + \lambda_m \left(-\frac{T u_T}{g_0 I_{sp}} \right) \quad (28)$$

The Hamiltonian for the lift-only or drag-only control methods can be computed by setting the drag or lift control variables to 1, respectively. For the hypersonic flight phase, the Hamiltonian is similar to the TDI altitude maximization problem with the same dynamics, and a Lagrangian term independent of control; the optimal control is bang-bang with the same switching functions as the TDI altitude maximization for all control methods.

For the propulsive descent, the thrust control, u_T, is linear with respect the Hamiltonian. The optimal control will be bang-bang by Pontryagin's Minimum Principle with the switching function as follows:

$$S = (\lambda_m - 1) \frac{T}{g_0 I_{sp}} + \lambda_V \frac{T}{m} \quad (29)$$

2.5 Linkage of Reachable and Controllable Terminal Descent Initiation States

Since the entry vehicle will enter the Martian atmosphere at some specified initial state and must land at another specified final state, there will be a set of reachable TDI states for which the vehicle can apply hypersonic flight control to reach a TDI state from the entry state and a set of controllable TDI states that the vehicle can initiate the propulsive descent stage to achieve the landing state. The two sets of TDI states do not necessarily intersect; it may not be possible to

achieve the landing state with a given entry state and system configuration. Examination of the intersection of the reachable and controllable sets can be a useful tool for mission design [12] as it is the subset of the TDI states for both the reachable and controllable sets that make a mission feasible. The intersection of the reachable and controllable sets is defined as the feasible set of TDI states.

An optimal control problem similar to the TDI altitude maximization was formulated to find the reachable TDI states to target a goal state. The cost function for this is a minimization of the normalized square residuals between the terminal hypersonic flight state and goal TDI state:

$$J = \left(\frac{V(t_f) - V_{goal}}{V_{goal}}\right)^2 + \left(\frac{\gamma(t_f) - \gamma_{goal}}{\gamma_{goal}}\right)^2 + \left(\frac{h(t_f) - h_{goal}}{h_{goal}}\right)^2 \tag{30}$$

To prevent singularities in the objective function for the target flight-path angle an arbitrary small value of 10^{-10} radians was used instead of zero. Singularities in the velocity and altitude terms were avoided as the state space did not include zero for these TDI target states. Control was changed to rate control of the bank angle and ballistic coefficient for lift control and drag control, respectively, to improve solution convergence. A bank angle rate limit of ±10° and ballistic coefficient rate limit of 100 kg/m^2/s were used. Limits on other states were similar to those for TDI altitude maximization in Section A, except for the final time. The final time constraint of 400 s was used for the drag-only control system and lift-and-drag control system.

The goal TDI states targeted by the objective function, Eq. (30), were TDI states in the precomputed, controllable set. Landing is constrained to occur at an altitude of 0 km and a 1 m/s velocity. Therefore, the controllable set are all set of TDI states for which the propulsive descent

can achieve this landing state. Furthermore, a constraint was placed so that the TDI altitude must be minimum to minimize thrust time while still achieving the landing state by assuming thrust was full throttle for the duration of the propulsive descent trajectory. Under these assumptions, computation of the controllable set becomes a root-finding problem. Given a TDI velocity and flight-path angle, there is only one TDI altitude that can achieve the landing state at full throttle thrust for the entire duration of the descent phase and constant thrust-to-weight ratio of 4. The propulsive descent trajectory was integrated using a fourth-order Runge-Kutta method to find the TDI altitude such that the final velocity and altitude were the desired landing conditions of 1 m/s and 0 km, respectively. The surface controllable TDI states resulting from the root-finding problem is shown in Fig 2.

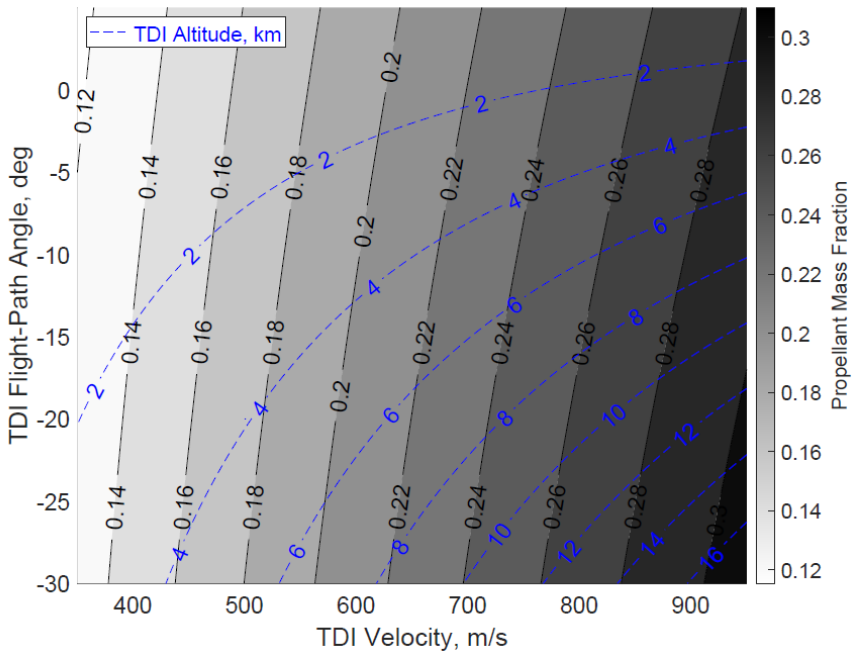

Fig 2. Surface of Controllable Set of TDI States for Propulsive Descent Phase

The objective function, Eq. (30), for hypersonic flight was applied to target the controllable TDI states shown in Fig 2. A threshold cost of 10^{-3} was set with any trajectory exceeding the threshold considered to have a final state sufficiently different from the target TDI state, resulting in an unreachable TDI state. A sample result of this analysis is shown in Fig 3 for a lift-only control. TDI states outside the red boundary are not reachable by the hypersonic control method. The TDI states are reachable by applying some hypersonic flight control, lift-only control in this case.

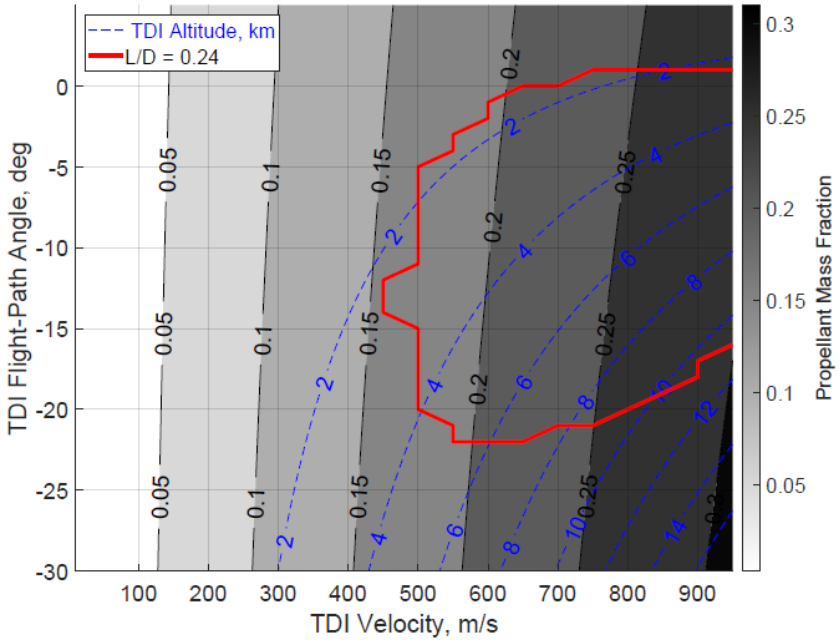

Fig 3. Reachable Set of TDI States for Lift-only Control at L/D of 0.24

CHAPTER 3: Maximizing Terminal Descent Initiation Altitude

3.1 Lift-only control TDI Altitude Maximization

Fig 4 shows the maximum TDI altitude and associated optimal control profile boundaries for the minimum ballistic coefficient (drag skirt deployed, $\beta = 225$ kg/m^2) vehicle configuration using lift-only control over various initial entry states. The control profile boundaries are given in terms of number of switches defined as the number of times the lift control variable crosses zero. The lift-up boundary indicates a transition from a one-switch lift reversal (from lift down to lift up) to lift-up-only control modes. The skip-out boundary is defined as initial conditions that yield trajectories where the vehicle passes above the initial altitude of 125 km. The two black dots in Fig 4 show the initial conditions of sample trajectories and control profiles in Fig 5 and Fig 6.

Fig 4 indicates the largest maximum TDI altitude is achieved at the largest initial velocities and moderate initial flight-path angles, approximately -19º to -21º. Initial flight-path angles tend to have a greater effect on the maximum TDI altitude than initial velocity. There are two primary optimal control profiles present over the range of initial conditions considered. Both control profiles are bang-bang as shown in the sample trajectories in Fig 5 and Fig 6. In this trajectory, a vertical L/D command of 0.24 corresponds to u_L=1 and a vertical L/D command of -0.24 corresponds to u_L=-1. At shallower flight-path angles, above the lift-up boundary, TDI altitude is maximized through entering the Martian atmosphere fully lift-down with a maneuver to fully lift-up at some point in the hypersonic portion of the trajectory. At steeper initial flight-path angles, the optimal solution is flight at full lift-up with no hypersonic maneuvers. This dependence on initial flight-path angle is due to the increased downward momentum of the vehicle and increased atmospheric density lower in the atmosphere. As shown by the equations of motion, Eq. (3)-(5),

lift-only control only affects the rate of change of the flight-path angle, and the magnitude of its effects are strongly dependent on the atmospheric density and vehicle velocity. At shallow initial flight-path angles, it is optimal to initially decreasing the flight-path angle with a lift-down entry in order to drop quickly into the lower atmosphere, maximizing the control authority provided by the larger atmospheric density and higher initial velocities. At steeper flight-path angles, the vehicle drops into the lower atmosphere quick enough that further decreasing the flight-path angle with a lift-down entry is detrimental to the final altitude, so a lift-up control profile must be used.

The maximum ballistic coefficient lift control option yields similar results with a lower maximum TDI altitude.

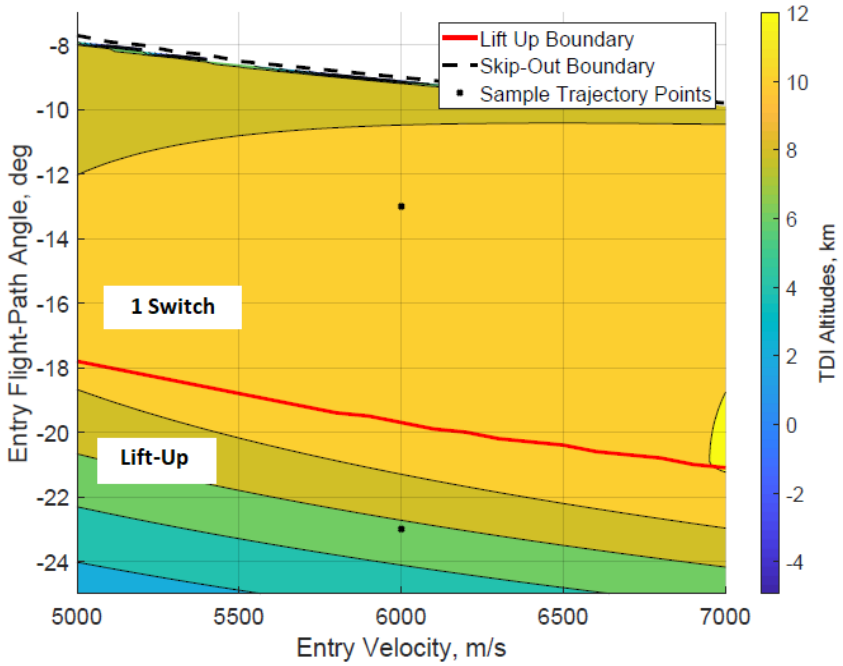

Fig 4. Lift-only Control, Maximum TDI Altitude over Various Entry Conditions

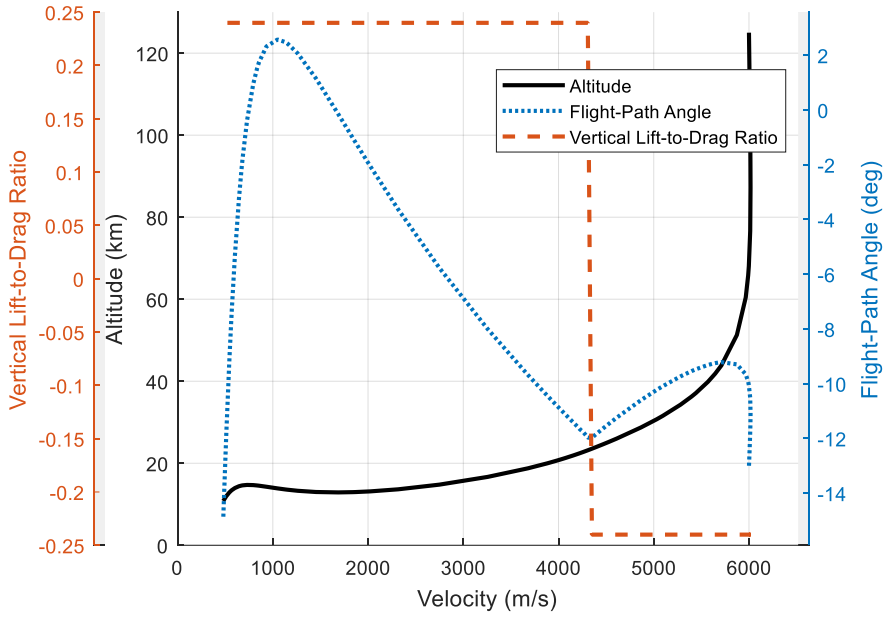

Fig 5. Lift-only Control, Sample One-Switch Lift Reversal Trajectory and Control Profile at V_0 = 6 km/s and γ_0 = -13º

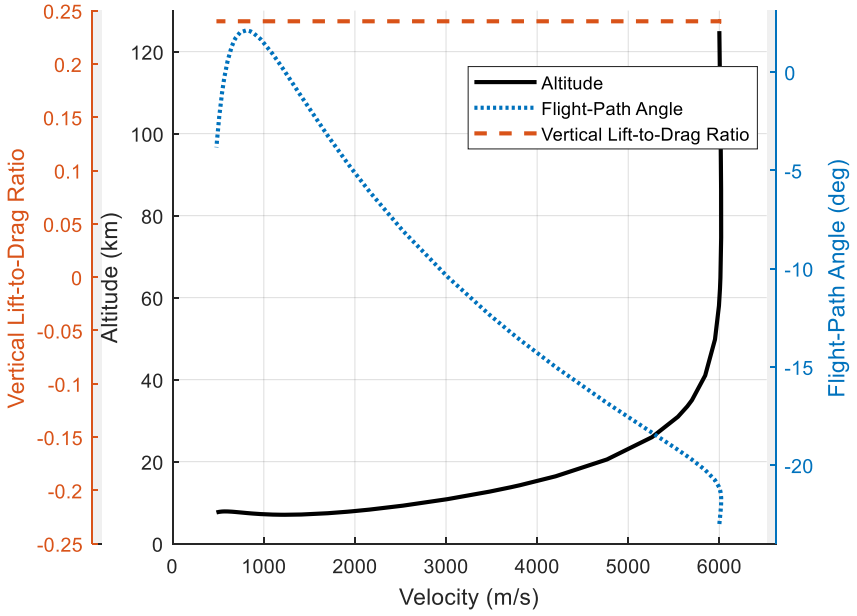

Fig 6. Lift-only Control, Sample Lift-up Trajectory and Control Profile at V_0 = 6 km/s and γ_0 = -23º

3.2 Drag Control TDI Maximum Altitude

Fig 7 shows the maximum TDI altitudes and their associated control profile boundaries over various initial entry conditions for a drag-only control system. The skip-out boundary shown occurs at steeper flight-path angles than the lift-only control case and corresponds to entry conditions that will result in a trajectory that passes above a 125 km altitude. The control profile boundaries are again defined in terms of changes in the optimal number of discrete switches in the drag command. Due to the bang-bang nature of the control profiles, optimal drag commands are always either minimum or maximum drag. Sample trajectories and control profiles as indicated on the Fig as black dots are shown in Fig 8 through Fig 11.

The maximum TDI altitude for drag-only trajectory control is larger at larger entry velocities and moderate flight-path angles. In contrast to lift-only trajectory control, there are four optimal bang-bang control profiles for drag-only control in this space. At the steepest entry flight-path angles, it is TDI-altitude optimal to have the drag skirt fully deployed at the minimum ballistic coefficient. As in the lift-only control case, this is due to a quick descent into the lower atmosphere caused by sufficient downward momentum at entry. Fig 8 shows a sample trajectory and control profile.

At moderate flight-path angles, enough of the vehicle's initial momentum points towards the planet that falling fastest is accomplished using a maximum ballistic coefficient to further decrease the flight-path angle while letting the magnitude of the momentum decrease less than it would at minimum ballistic coefficient. At shallower flight-path angles, too much momentum points horizontally, so it is beneficial to dissipate this horizontal energy by flying at a minimum ballistic coefficient before switching to a maximum ballistic coefficient to decrease the flight-path angle rate once the flight-path angle rate increases too much. This leads to the one and two-switch

optimal control profiles shown in Fig 7. Below the one-switch control boundary, a switch from maximum to minimum ballistic coefficient is optimal while above it a two-switch mode from minimum to maximum back to minimum ballistic coefficient is optimal. Example trajectories and control profiles of the one-switch and two-switch cases are shown in Fig 9 and Fig 10, respectively.

At the shallowest entry flight-path angles, a four-switch control profile maximizes the TDI altitude. A sample trajectory and control profile of this case is shown in Fig 11. The four-switch control profile is a special case of the two-switch case. Four-switch control profiles become optimal when a large lofting period exists. The goal of the initial phase of the optimal trajectories is always to reach the lower atmosphere quickly to maximize the contribution of control authority at higher velocities; therefore, to avoid a long loft or skip-out, the vehicle must dissipate energy by switching to minimum ballistic coefficient. The four-switch case can then be seen as a two-switch case with an extra two switches to avoid a long loft period.

At lower entry velocities and the shallowest entry flight-path angles, a three-switch control profile also exists. The three-switch control profile has low enough horizontal momentum that it no longer needs the initial momentum dissipation of the two-switch and four-switch cases but still needs the extra two switches to avoid long lofts. A sample trajectory and control profile of this three-switch case is shown in Fig 12. Along the boundary between the three-switch and four-switch optimal control profiles, a small region of five-switch profiles exists. The five-switch control profile resembles a three-switch case with a quick starting at maximum ballistic coefficient with a short duration switch to minimum ballistic coefficient before switching back to maximum ballistic coefficient. A sample trajectory and control profile of this case is shown in Fig 13.

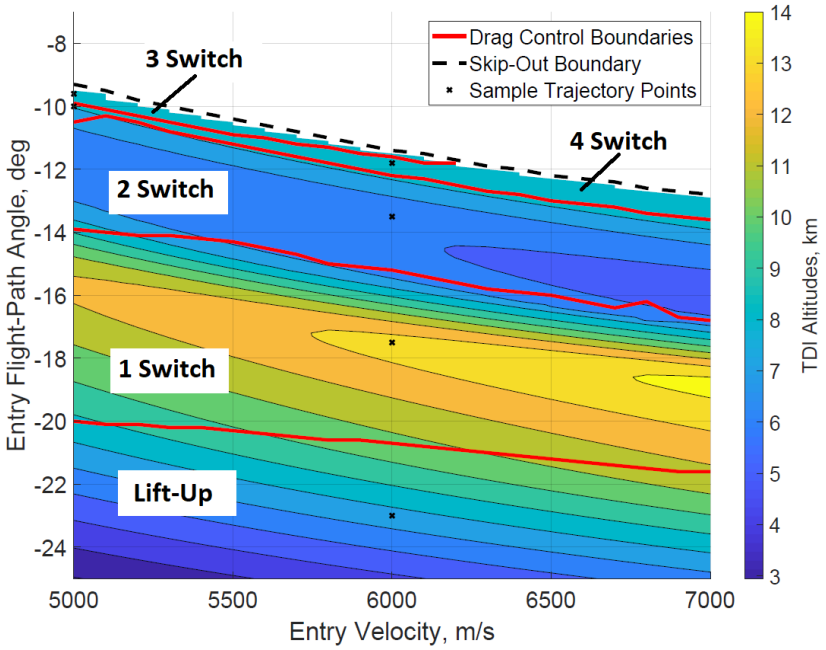

Fig 7. Drag-only Control, Maximum TDI Altitude over Various Entry Conditions

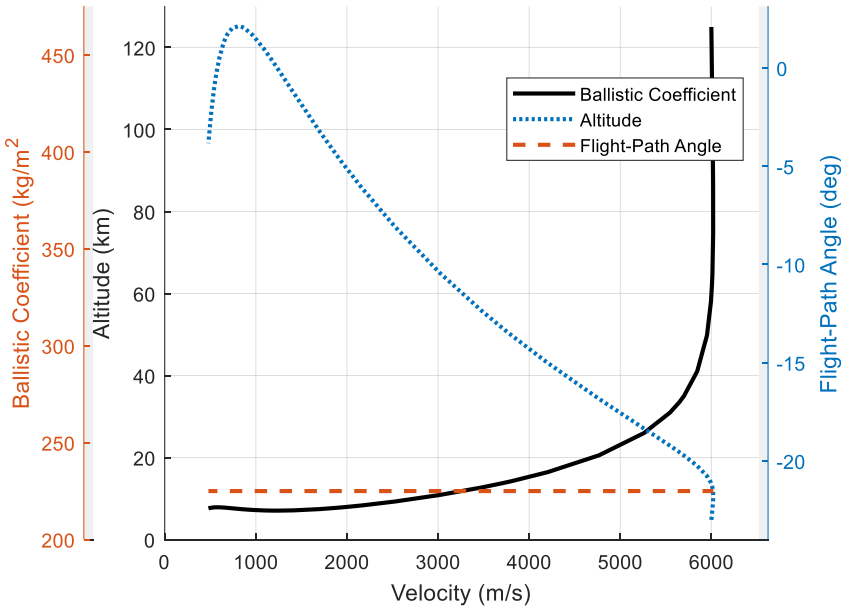

Fig 8. Drag-only Control, Sample Minimum Ballistic Coefficient Trajectory and Control Profile at V_0 = 6 km/s and γ_0 = -23°

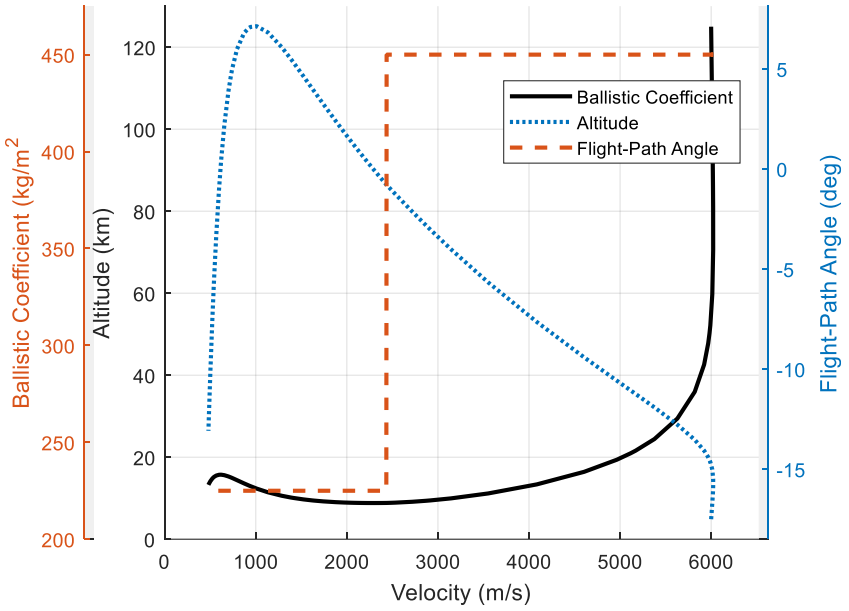

Fig 9. Drag-only Control, Sample One-switch Trajectory and Control Profile at V_0 = 6 km/s and γ_0 = -17.5º

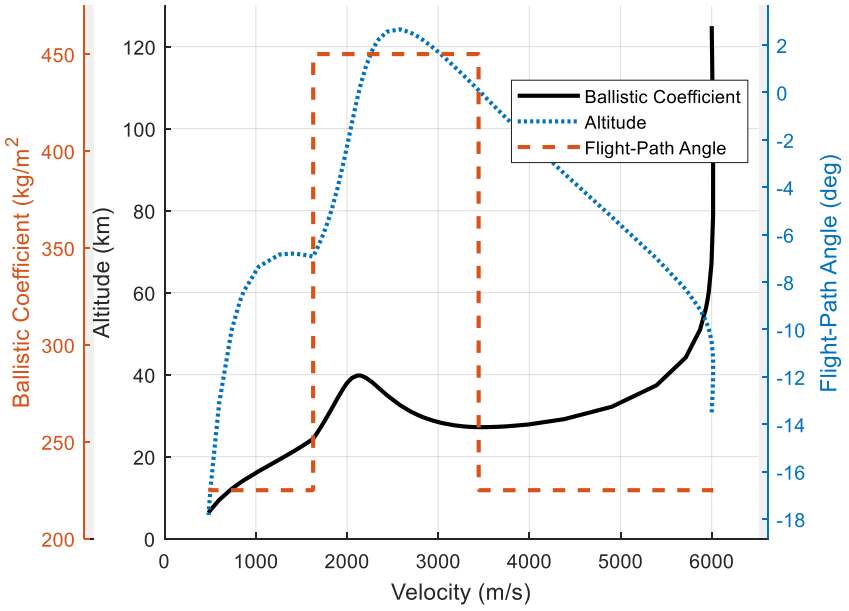

Fig 10. Drag-only Control, Sample Two-Switch Trajectory and Control Profile at V_0 = 6 km/s and γ_0 = -13.5º

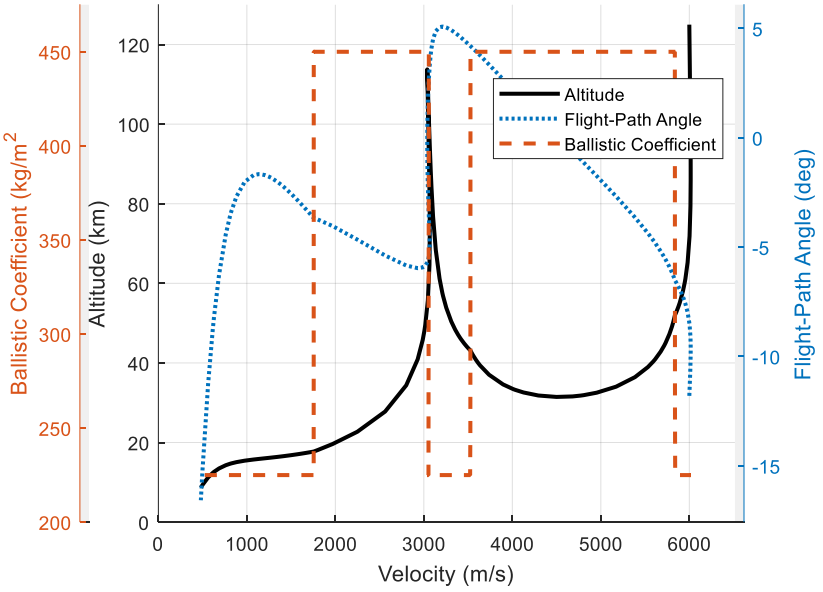

Fig 11. Drag-only Control, Sample Four-switch Trajectory and Control Profile at V_0 = 6 km/s and γ_0 = -11.8º

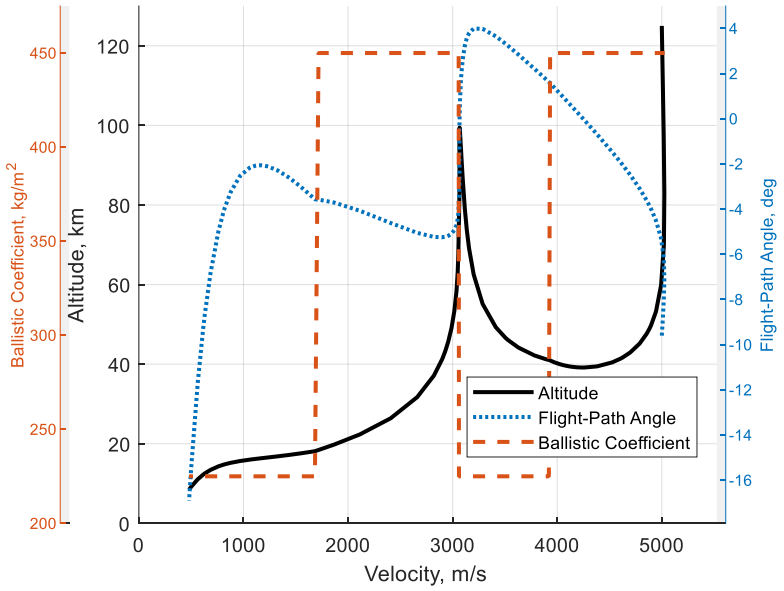

Fig 12. Drag-only Control, Sample Three-switch Trajectory and Control Profile at V_0 = 5 km/s and γ_0 = -9.6º

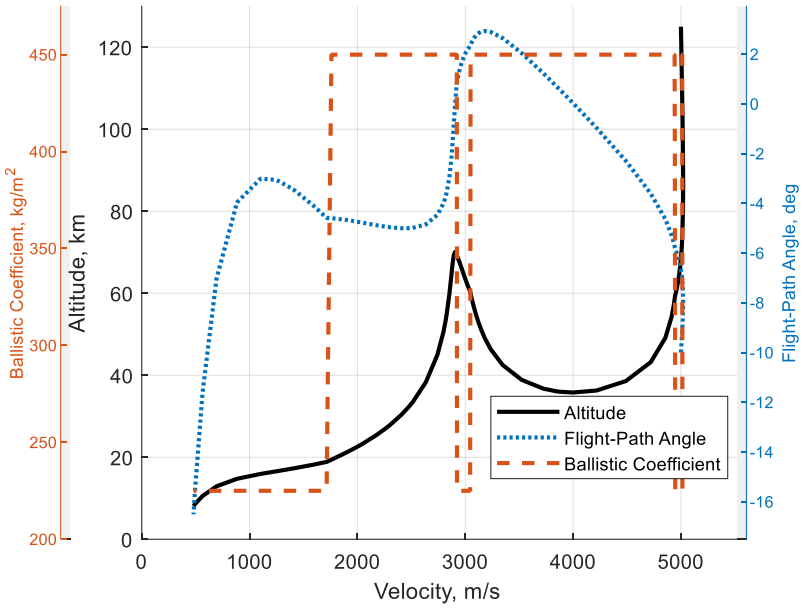

Fig 13. Drag-only Control, Sample Five-switch Trajectory and Control Profile at V_0 = 5 km/s and γ_0 = -10.0º

3.3 Lift-and-Drag Control TDI Altitude Maximization

Fig 14 shows the maximum TDI altitudes and associated control profile boundaries obtained at various entry conditions for a lift-and-drag control system. Qualitatively, results appear similar to those of lift-only control system with two optimal control profiles existing for the lift portion of the lift-and-drag control. However, there are fewer optimal control profiles for the drag portion of lift-and-drag control than the drag-only control system. Further, the lift-up boundary and minimum ballistic coefficient boundaries do not occur at the same initial conditions relative to the lift-only control case; therefore, there is also a region between these boundaries where a drag-only control system with lift-up would be optimal. A sample trajectory and control profile in this region, at an entry velocity of 6 km/s and entry flight-path angle of -19º, is shown in Fig 15. Below this region an always lift-up, minimum ballistic coefficient control profile is optimal to maximize TDI

altitude, and above this region, a combination of lift and drag control is optimal. Sample trajectories and control profiles in these two regions are shown in Fig 16 and Fig 17, respectively.

At the shallowest entry flight-path angles, the three-switch and four-switch drag control profiles seen in the drag-only control are not optimal for the lift-and-drag control. The three-switch and four-switch cases were special cases to avoid long lofting near-skip-out in the drag-only control system and are no longer necessary because of the inclusion of the lift-down option of lift control; the vehicle uses a lift-down control command to avoid skip-out at entry conditions that would lead to skip-out for drag-only control systems. A sample trajectory and control profile of this case is shown in Fig 18.

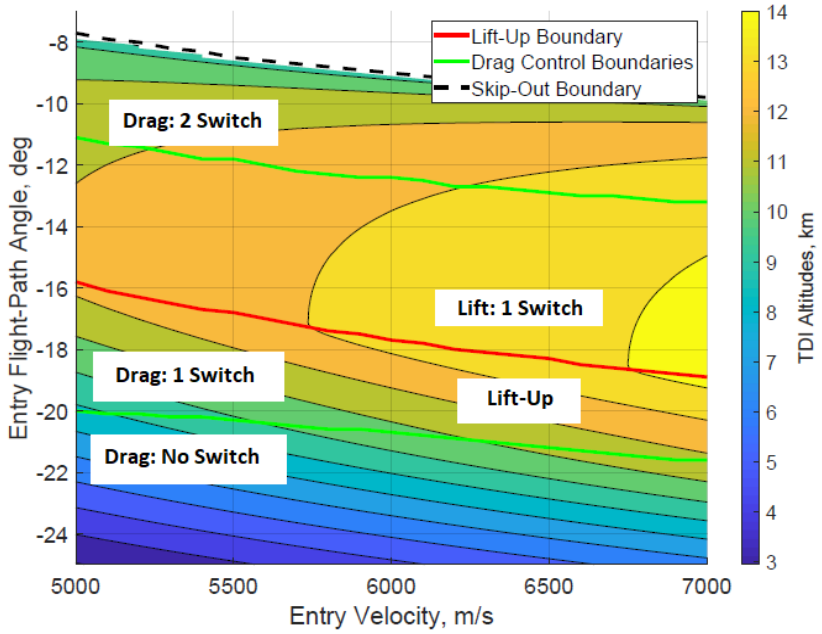

Fig 14. Lift-and-Drag Control, Maximum TDI Altitude over Various Entry Conditions

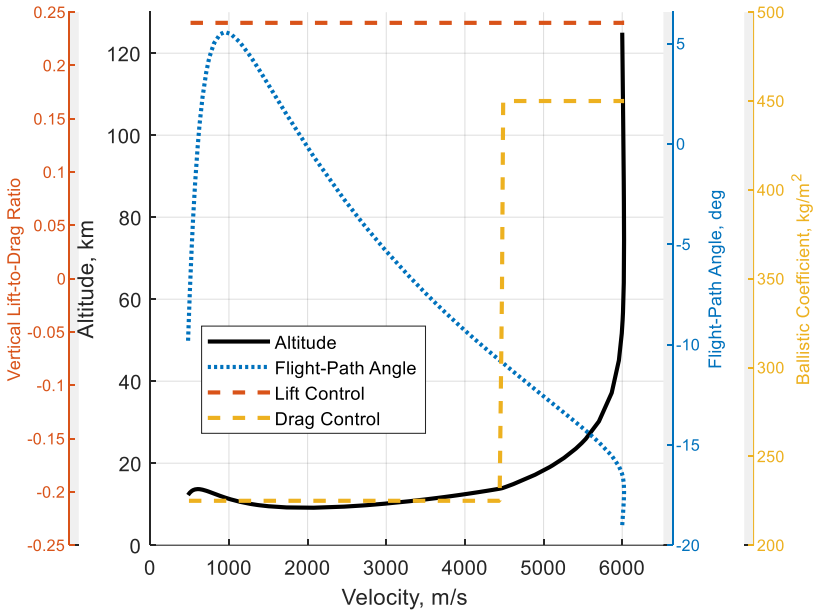

Fig 15. Lift-and-Drag Control, Sample Trajectory and Control Profile at Entry Conditions of V_0 = 6 km/s and γ_0 = -19.0º

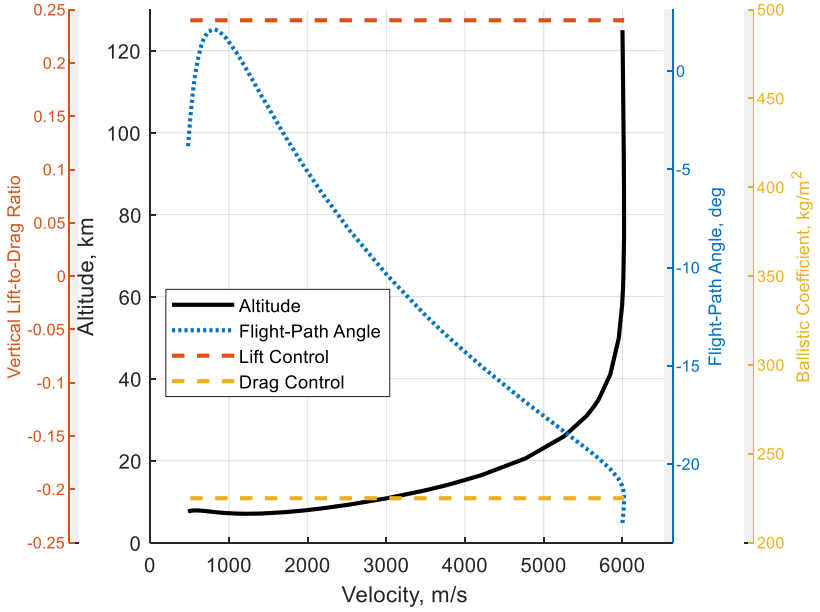

Fig 16. Lift-and-Drag Control, Sample Trajectory and Control Profile at Entry Conditions of V_0 = 6 km/s and γ_0 = -23.0º

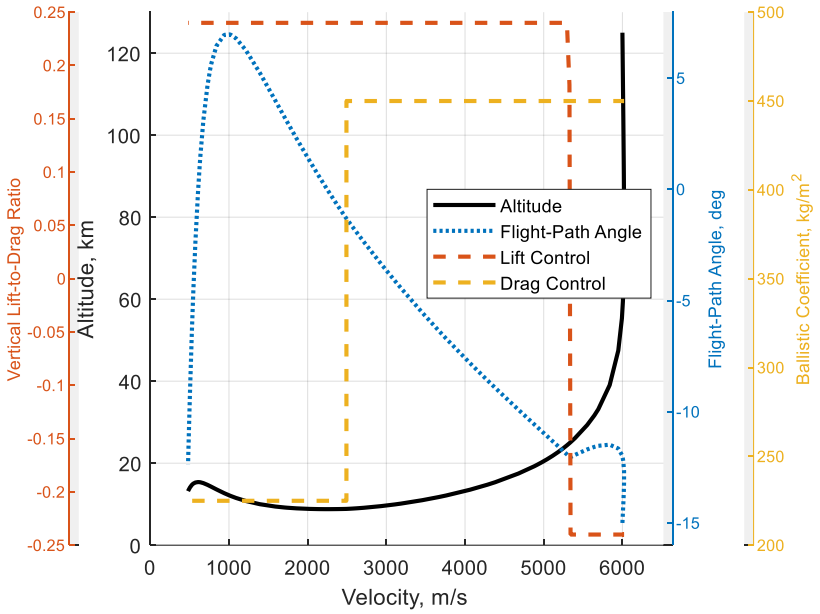

Fig 17. Lift-and-Drag Control, Sample Trajectory and Control Profile at Entry Conditions of V_0 = 6 km/s and γ_0 = -15.0º

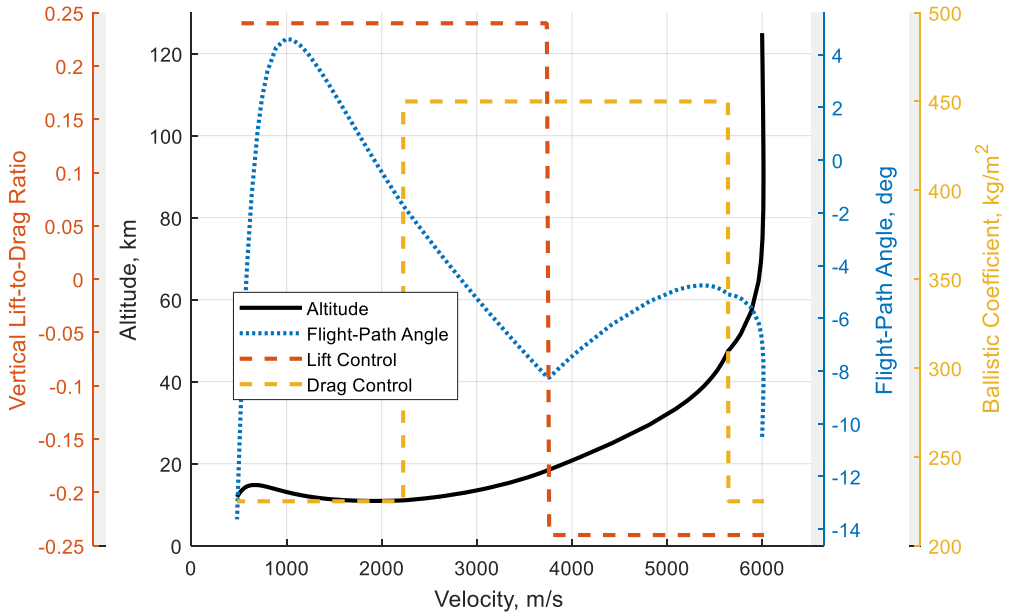

Fig 18. Lift-and-Drag Control, Sample Trajectory and Control Profile at Near-Skip-Out Entry Conditions of V_0 = 6 km/s and γ_0 = -10.5º

3.4 TDI Altitude Maximization Control Method Comparison

Drag control differs from lift control as it directly effects both the rate of the momentum's magnitude, velocity, and rate of the momentum's direction, flight-path angle, while lift control only effects the rate of the momentum's direction as shown by the drag control variables inclusion in the dynamic equations, Eq. (3) and Eq. (4) . To maximize TDI altitude, it is always beneficial to initially drop deep into the atmosphere quickly, minimizing the rate of change in altitude, and then turn upwards at the end of the trajectory. Above the lift-up boundary, lift control always accomplishes these two phases with a lift-down entry and switch to lift-up at the end of the trajectory; however, drag control may accomplish the initial minimization of altitude rate of change differently depending on the vehicle's initial momentum and whether it is more important to decrease velocity or flight-path angle. From Eq. (3)-(4), a larger ballistic coefficient leads to a larger velocity rate but lower flight-path angle rate while the opposite is true for a smaller ballistic coefficient.

The difference in maximum TDI altitudes of a lift-and-drag control system versus the lift-only control system at constant, minimum ballistic coefficient, respectively, and all control profile boundaries associated with the two methods are shown in Fig 19. A positive difference corresponds to a higher maximum TDI altitude in the lift-and-drag control. Both the lift and drag control boundaries for the lift-and-drag control are plotted as dotted lines with the lift-up boundary in red and the drag control boundaries in green. The lift-only, lift-up boundary is plotted in solid red. All control boundaries are as defined in previous sections.

As shown in Fig 19, the lift-and-drag control system always yields a greater maximum TDI altitude above the drag control boundary of the lift-and-drag control system at the steepest initial flight-path angle. At the steepest initial flight-path angles, both systems are identical and there is

no benefit to the lift-and-drag control system. The lift-up boundary of the lift-and-drag control system occurs at shallower initial flight-path angles than the lift-only control system for all initial velocities. The difference between these two options are a varying ballistic coefficient, between 450 kg/m^2 and 225 kg/m^2 in the lift-and-drag control case and a constant ballistic coefficient, 450 kg/m^2 in the lift-only case. While Lorenz and Putnam found that a constant ballistic coefficient does not significantly affect the lift-up boundary [17], this appears to not hold when the ballistic coefficient is allowed to vary during hypersonic flight. Below both lift-up boundaries there is a small region, above the lower drag control boundary of the lift-and-drag system, where the lift-and-drag control uses purely drag control; however, in this region, the difference between the maximum TDI altitude of both system, gradually goes to zero with a steeper entry flight-path angle. Below the lower drag control boundary of the lift-and-drag system, both systems are identical, flying lift-up at minimum ballistic coefficient for the duration of their trajectories.

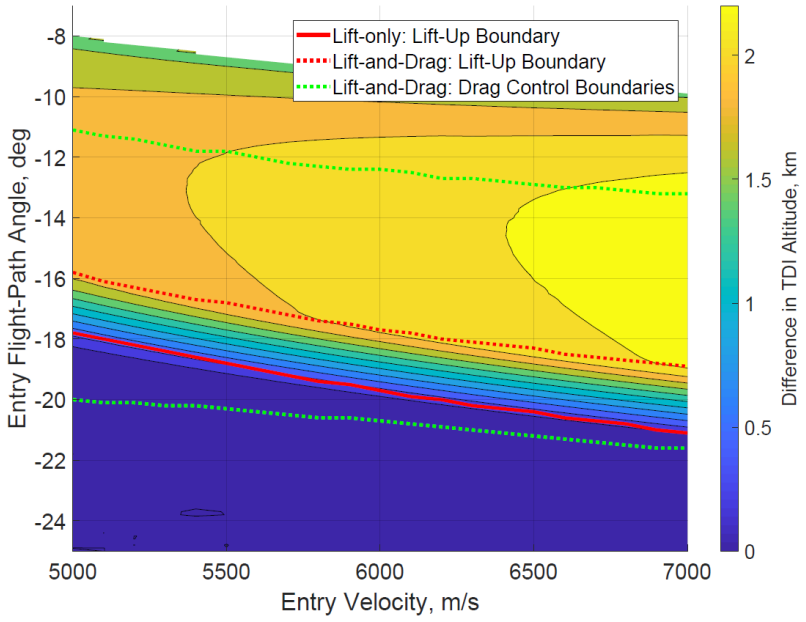

Fig 19. Difference of Maximum TDI Altitude between Lift-and-Drag Control and Lift-only Control.

Fig 20 shows the difference in maximum TDI altitude between the lift-and-drag control system and the drag-only control system and all associated control boundaries over various entry conditions. The lift-and-drag control boundaries are plotted as dotted lines with the lift-up boundary in red and the drag control boundaries in green. The drag-only control boundaries are plotted in solid green. All control boundaries are as defined in previous sections.

The lift-and-drag control system again yields a greater maximum TDI altitude than the drag-only system at shallower initial flight-path angles. This contrasts with the more modest gains shown by lift-and-drag control over lift-only control in Fig. 12. The drag control boundary of the lift-and-drag system at the shallowest initial flight-path angles occurs at larger initial flight-path angles than the drag-only control option. Above this boundary a two-switch drag control mode is optimal while below it, a one-switch control mode is optimal. Because the two-switch drag control profiles yields a lower maximum TDI altitude, this higher boundary in the lift-and-drag control system leads to the increased maximum TDI altitudes in the lift-and-drag control system between the two control boundaries. Below the lift-up boundary of the lift-and-drag system, both vehicles fly using only drag control with similar maximum TDI altitudes. The drag control boundary at the steepest initial flight-path angle, separating the one-switch and no-switch control profiles, for both control methods are identical.

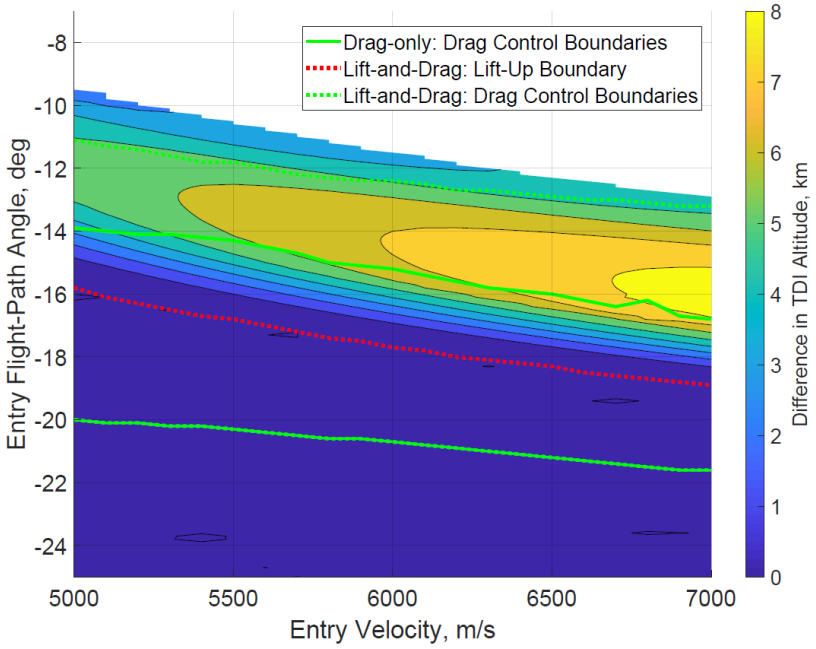

Fig 20. Difference of Maximum TDI Altitude between Lift-and-Drag Control and Drag-only Control.

Fig 21 shows the difference in maximum TDI altitude of lift-only control versus drag-only control at various entry conditions with positive values signifying a higher maximum TDI altitude in the lift-only control system. As shown, there are distinct regions where either control method has an advantage. Above the red, dashed line, the lift-only control method yields a larger maximum TDI altitude; below the red, dashed line, drag control provides an advantage. Below the lift-only, lift-up boundary, the advantage provided by drag control gradually decreases until below the red, solid line where both vehicles fly identically controlled trajectories, lift-up at minimum ballistic coefficient. Differences in maximum TDI altitude below the solid, red line are less than 1 m.

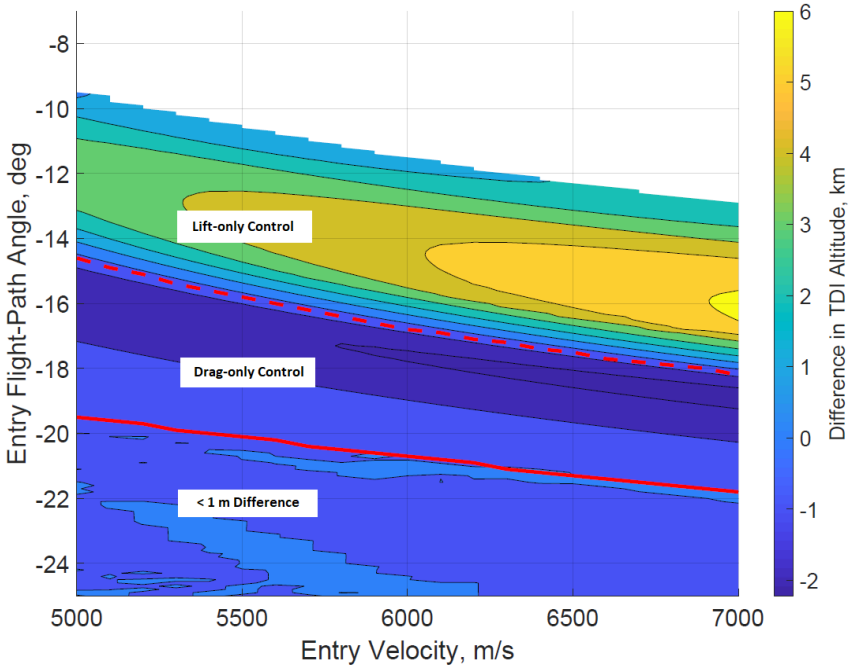

Fig 21. Difference of Maximum TDI Altitude of Lift-only Control and Drag-only Control

CHAPTER 4: Propellant Mass Fraction Minimization

While TDI altitude maximization is an important metric for parachute descent systems, for propulsive descent, a more important parameter to minimize is the propellant mass fraction which allows for a larger payload mass. A two-phase optimal control problem as described in CHAPTER 2: Section 2.4 was used to evaluate each of the three control methods' ability to minimize the PMF.

4.1 Lift-only Control PMF Minimization

The minimum PMF of the lift-only control method at minimum ballistic coefficient and the control profile boundary, the lift-up boundary, over various entry velocities and flight-path angles is shown in Fig 22. The skip-out boundary is defined as the entry conditions above which the vehicle trajectory passes above a 125 km altitude. The lift-up boundary divides trajectories with a one-switch control profile, above the boundary, and a no-switch, lift-up control profile, below the boundary. Initial conditions for sample hypersonic flight trajectories and control profiles, shown in Fig 23 and Fig 24, are indicated by black dots in Fig 22.

As shown in Fig 22, a larger initial velocity and steeper initial flight-path angle leads to a lower minimum PMF. The optimal lift-only control profile trends for PMF minimization are similar to the TDI altitude maximization optimal control profile trends with all optimal control being bang-bang; however, the majority of the design space for PMF minimization has a one-switch control mode, starting at lift-down entry with a switch to lift-up. A sample trajectory of this control profile at an entry velocity of 6 km/s and entry flight-path angle of -16º is shown in Fig 23 with the red, dashed line dividing the hypersonic flight and propulsive descent phases. There is also a small region on the design space at low entry velocities and steep flight-path angles where a no-switch, lift-up control mode is minimizes the PMF. Similar to TDI altitude maximization,

quickly dropping into the lower atmosphere with a final turn upwards through a lift-up switch minimizes the PMF in most cases. For PMF minimization, the lift-up boundary occurs at lower initial flight-path angles. The lift-up boundary likely only exists here to prevent an unrecoverable fall.

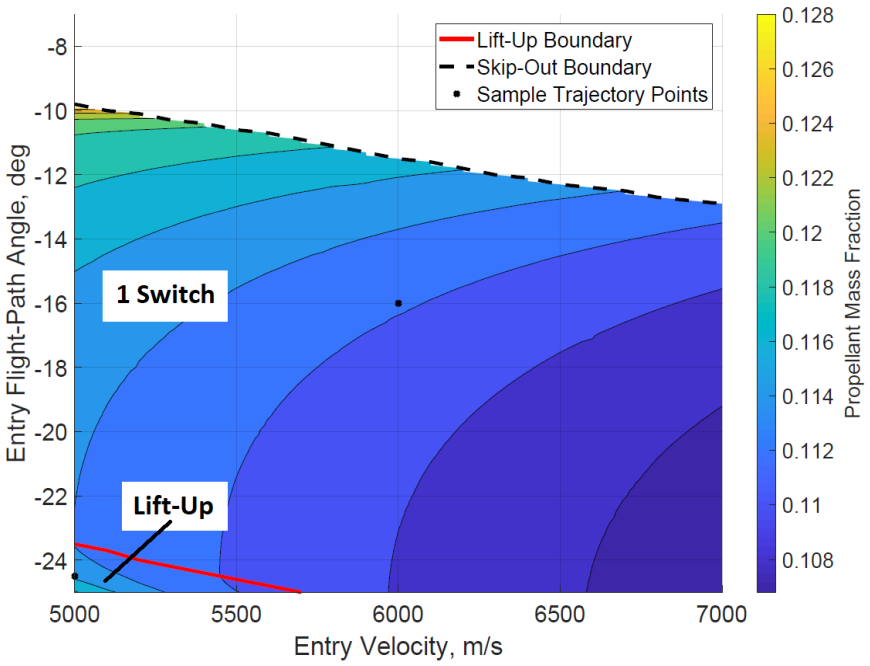

Fig 22. Lift-only Control, Minimum PMF over Various Entry Conditions

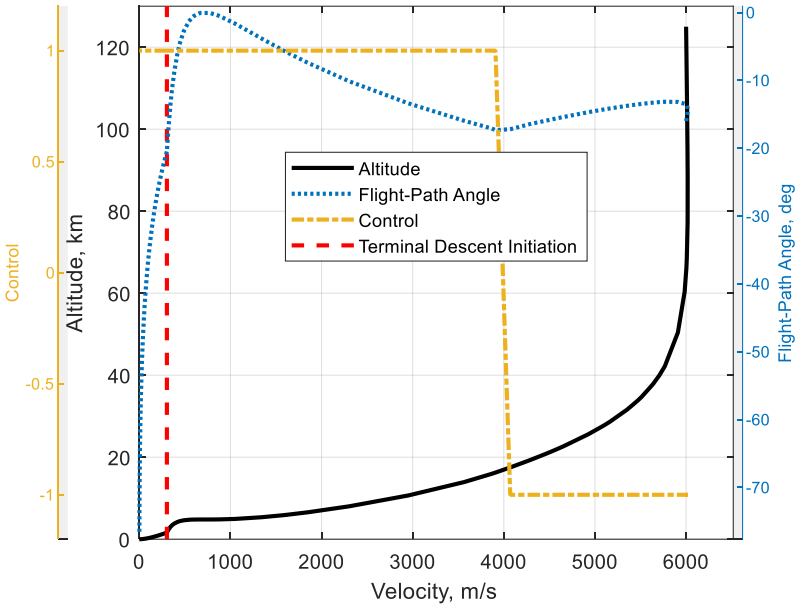

Fig 23. Lift-only Control, Sample One-Switch Trajectory and Control Profile at V_0 = 6 km/s and γ_0 = -16º

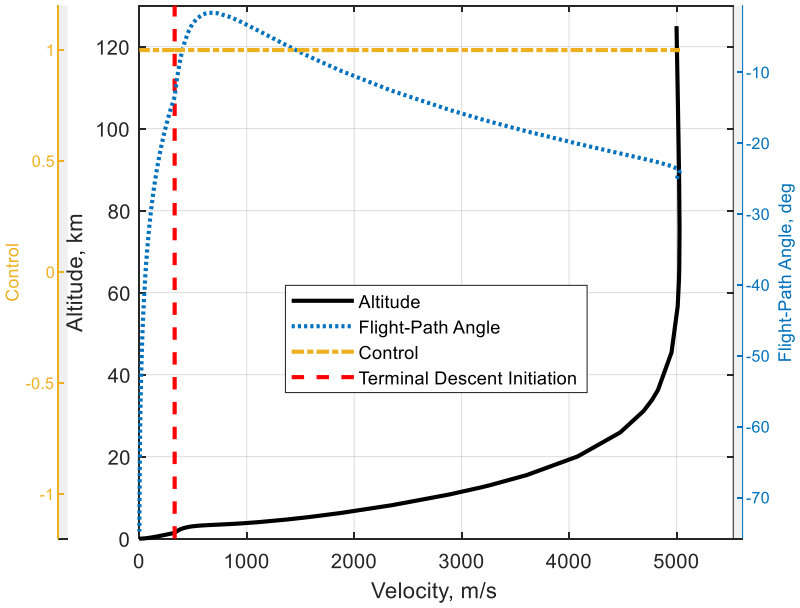

Fig 24. Lift-only Control, Sample No-Switch Trajectory and Control Profile at V_0 = 5 km/s and γ_0 = -24.5º

4.2 Drag-only Control PMF Minimization

Results for minimizing the PMF using drag-only control and the associated optimal control profile boundaries over various entry conditions are shown in Fig 25. Sample trajectory and control profile points are indicated by black dots. There are three bang-bang optimal control profiles for this method. At the steepest entry flight-path angles, a one-switch control profile was found to be optimal. This control profile was associated with the smallest minimum PMFs, especially at the largest entry velocities. A sample trajectory and control profile of this case is shown in Fig 26. The hypersonic control profile in Fig 26 is in terms of the drag control variable with a value of 1 corresponding to a maximum ballistic coefficient of 450 kg/m^2 and a value of 2 corresponding to minimum ballistic coefficient of 225 kg/m^2. The propulsive descent control is in terms of the thrust control variable from ignition off, 0, to full throttle, 1. All control profiles in this case start with a maximum ballistic coefficient with a switch to minimum ballistic coefficient towards the end to the trajectory, similar to the one-switch case seen in the TDI altitude maximization results.

At shallower entry flight-path angles, a two-switch control profile is PMF-optimal and associated with larger minimum PMF values than the one-switch control profiles. A sample trajectory and control profile of this case at an entry velocity of 6 km/s and entry flight-path angle of -22.5º is shown in Fig 27. While the control does not look strictly bang-bang in the velocity domain of Fig 27, control switch commands are instantaneous in the time domain. All control profiles in this region begin at minimum ballistic coefficient with a switch to maximum ballistic coefficient before switching back to minimum ballistic coefficient.

At entry flight-path angles closest to the skip-out boundary, a four-switch control profile is PMF optimal. A sample trajectory and control profile at an entry velocity of 6 km/s and entry flight-path angle of -12.5º is shown in Fig 28. Like for the TDI maximization, the four-switch,

drag-only control profile is a special case of the two-switch optimal control profile where the vehicle switches to a minimum ballistic coefficient to dissipate energy to avoid a large lofting period. By doing this, the vehicle enters the lower atmosphere quicker.

Results for PMF minimization, drag-only control are similar to the TDI altitude maximization; however, the no-switch, minimum ballistic coefficient region and three-switch optimal control profile cases were not seen for the PMF minimization. It is possible that these cases do exist but exist at lower entry flight-path angles and lower entry velocities than examined. This scenario is likely as the lift-only control saw a much lower lift-up boundary for PMF minimization than for the TDI altitude maximization.

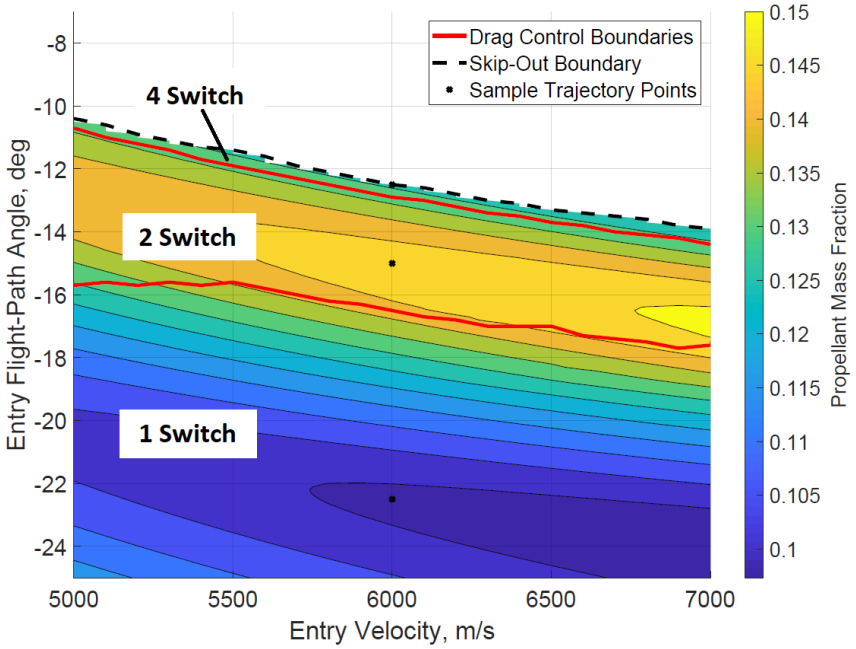

Fig 25. Drag-only Control, Minimum PMF over Various Entry Conditions

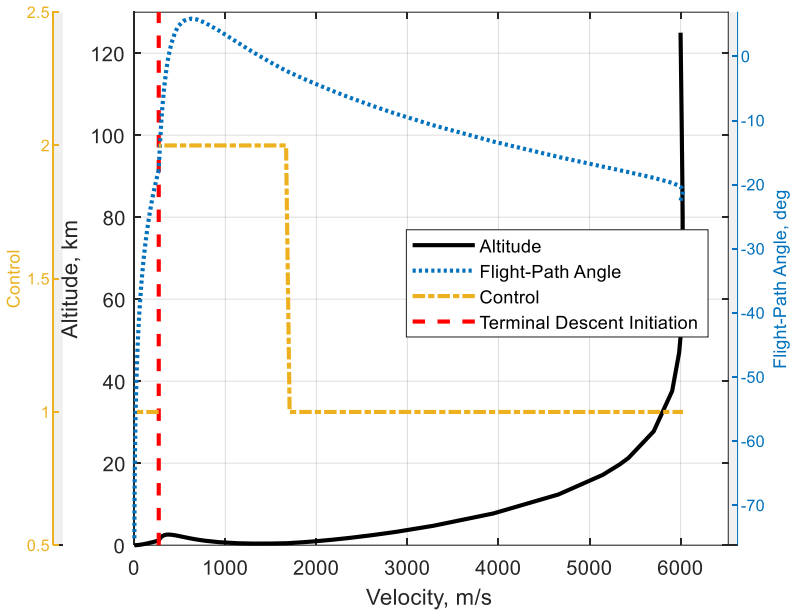

Fig 26. Drag-only Control, , Sample One-Switch Trajectory and Control Profile at V_0 = 6 km/s and γ_0 = -22.5º

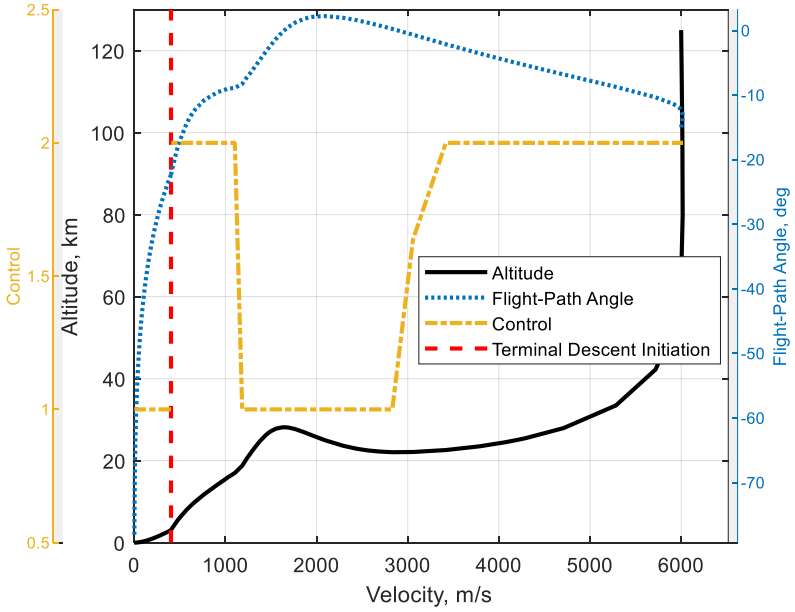

Fig 27. Drag-only Control, Sample Two-Switch Hypersonic Trajectory at V_0 = 6 km/s and γ_0 = -15º

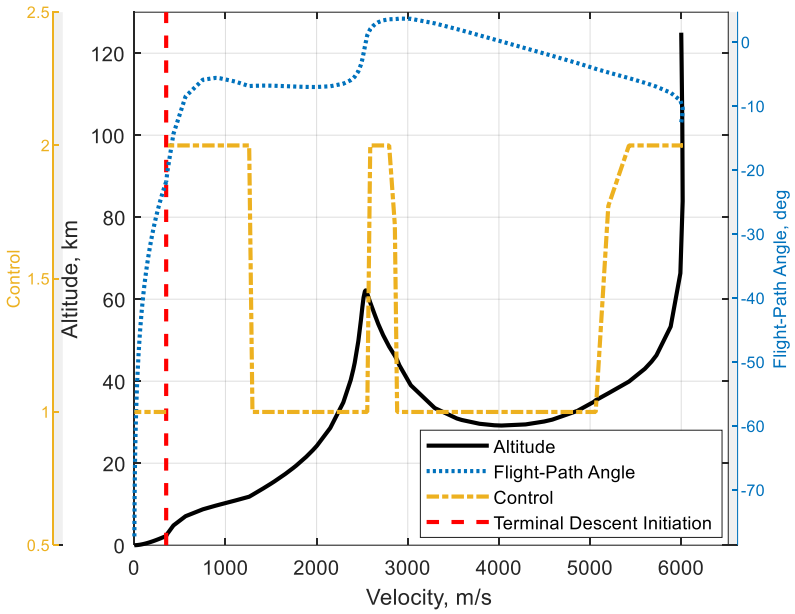

Fig 28. Drag-only Control, Sample Four-Switch Hypersonic Trajectory at V_0 = 6 km/s and γ_0 = -12.5°

4.3 Lift-and-Drag Control PMF Minimization

The minimum PMF and associated lift and drag control boundaries for the lift-and-drag control method over various entry conditions are shown in Fig 29. All control profiles were again found to be bang-bang. Similar to the lift-only control case, the lift control of the lift-and-drag system has two optimal control profiles. At the steepest entry flight-path angles, a no-switch lift-up control profile is PMF-optimal; however, this control profile results in a larger minimum PMF as the entry flight-path angle decreases. At entry flight-path angles above the lift-up boundary, a one-switch lift control mode is PMF optimal. This case for lift-and-drag control is similar to the lift-only case, entering the atmosphere with the lift vector pointed fully down and a switch to lift-up at some point in the trajectory; however, the inclusion of drag control enlarges the lift-up optimal control region by increasing the entry flight-path angles that the lift-up boundary occurs

at. At the largest entry velocities and flight-path angles, optimal control profiles of various switches were found to result in similar minimum PMFs and time-of-flights, making it difficult for the optimal control solver to find the true optimal control to minimize PMF solution. This similarity in various control profiles was thought to be the cause of the in the slight “bump” in the lift-up boundary at large entry velocities.

The drag control for the lift-and-drag control method has only two optimal control profiles. The four-switch mode seen in the drag-only control was not present for lift-and-drag control, likely for the same reasons it was not seen in the lift-and-drag control TDI altitude maximization; the lift-down command decreases lofting enough for a four-switch control to be unnecessary. All entry flight path angles below the drag control boundary, including those below the lift control boundary, result in a one-switch drag control profile. Above the drag control boundary, a two-switch control mode is PMF optimal. The control profiles for these two regions are similar to the drag-only control method. Both have a switch from maximum to minimum ballistic coefficient towards the end of the trajectory with the difference between the two being a switch from minimum to maximum ballistic coefficient towards the start of the trajectory in the two-switch control mode.

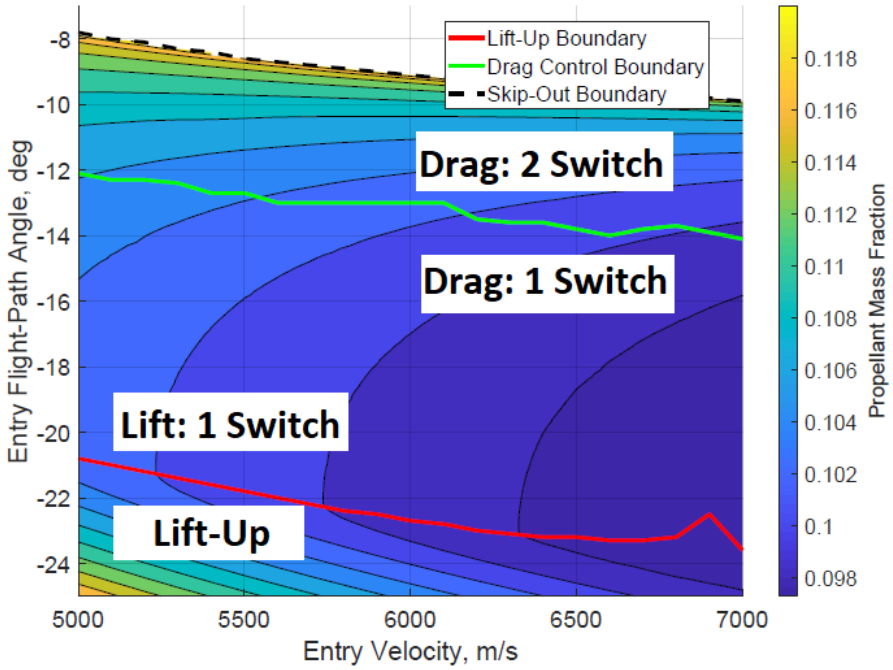

Fig 29. Lift-and-Drag Control, Minimum PMF over Various Entry Conditions

4.4 Minimum PMF Control Method Comparison

Fig 30 shows the difference in minimum PMF over the various entry conditions for the lift-only control method and lift-and-drag control method, respectively. A positive value indicates a lower minimum PMF in the lift-and-drag control method. Lift and drag control boundaries are as defined in prior sections with the lift-up boundary of the lift-only system plotted in solid red and lift and drag control boundaries of the lift-and-drag system plotted in red and green, respectively, as dotted lines. The inclusion of both lift and drag modulation reduces the required PMF by approximately 0.01 or 10.3% difference for most entry conditions with a larger reduction at lower entry velocities and shallower entry flight-path angles. The difference in PMF gradually is reduced below the lift-up boundary of the lift-and-drag system until below the lift-only, lift-up boundary where the systems are identical, lift-up, one-switch drag control. Fig 30 also shows that the

inclusion of both lift and drag modulation increases the lift-up control region as the lift-up boundary occurs at shallower flight-path angles for the lift-and-drag control method than the lift-only method.

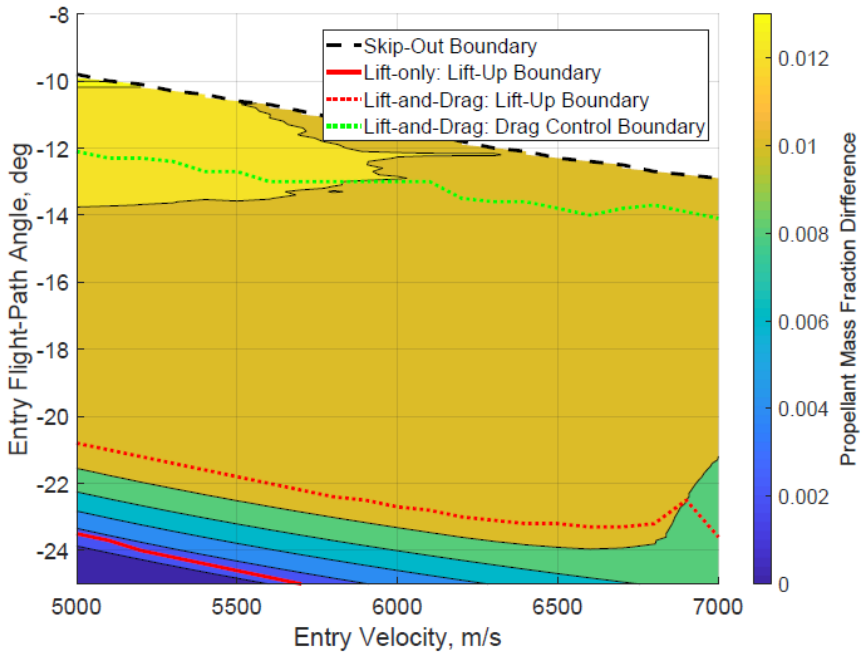

Fig 30. Difference in Minimum PMF between Lift-only and Lift-and-Drag Methods

The difference in minimum PMF between the lift-and-drag and drag-only control methods and all associated control boundaries over various entry conditions are shown in Fig 31. Positive PMF differences indicate a lower minimum PMF in the lift-and-drag control method. The lift-and-drag control boundaries are plotted as dotted lines with the lift-up control boundary plotted in red and the drag control boundary plotted in green. The drag-only, drag control boundaries are plotted as a solid green line. The control boundaries are as previously defined. The drag control boundary of the lift-and-drag system, separating the two-switch and one-switch optimal control profiles, occurs at a similar location as the drag-only, drag control boundary separating the two-switch and four-switch control modes. The drag control boundary of the lift-and-drag system rises above the

skip-out boundary as the lift-and-drag control system skips-out at a shallower entry flight-path angle than the drag-only control system. The skip-out boundary shown in Fig 31 is that of the drag-only system rather than the lift-and-drag system; the entry conditions between the two skip-out boundaries would be possible only for the lift-and-drag system.

Fig 31 shows the greatest benefit of including both lift and drag modulation is achieved at shallow entry flight-path angles and higher entry velocities; however, there is always a benefit above the lift-up boundary of the lift-and-drag system. Below the lift-up boundary of the lift-and-drag, the two methods are identical, lift-up, one-switch drag modulation.

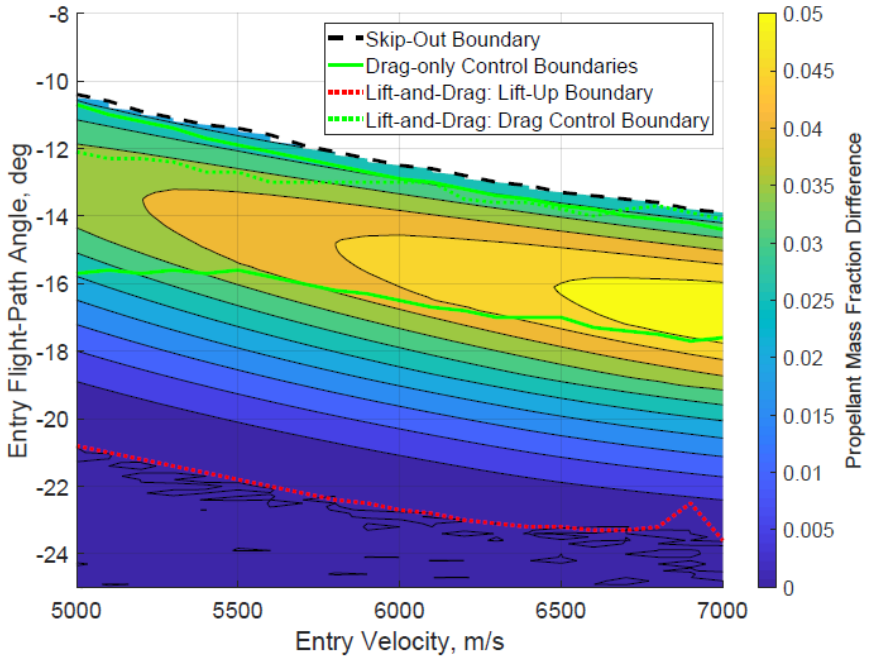

Fig 31. Difference in Minimum PMF between Drag-only and Lift-and-Drag Control Methods

The difference between drag-only and lift-only minimum PMF over various entry conditions are shown in Fig 32. A positive difference in PMF indicates a reduction in minimum PMF by choosing the drag-only control method. At steep entry flight-path angles, the drag-only

method leads to a lower minimum PMF while at shallow entry flight-path angles, the lift-only method is superior. The optimal lift-only control PMF value does not occur at shallow entry flight-path angles. Both the lift-only and drag-only control methods achieve an optimal PMF trajectory at higher entry velocities and steeper entry flight-path angles. For the notional lift-only and drag-only vehicle configurations chosen, the drag-only control system achieves a lower optimal PMF magnitude of 0.0974 than the lift-only control system optimal PMF magnitude of 0.1068. While drag-only control may lead to a lower PMF, entering the atmosphere at a steep flight-path where it is better than lift-only control may not be feasible due to an increased heat rate and deceleration.

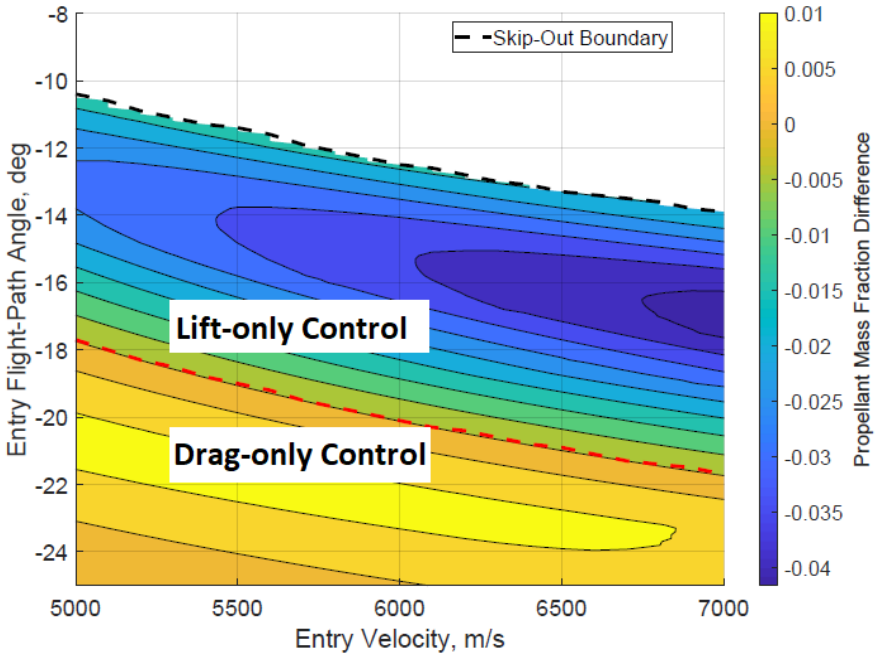

Fig 32. Difference in Minimum PMF between Lift-only and Drag-only Control Methods

To explore the trade between lift and drag modulation to minimize PMF, the vertical lift-to-drag ratio and ballistic coefficient ratios were varied for a lift-and-drag system with nominal entry condition specified in Table 2. Fig 33 shows the results of this trade. A vertical lift-to-drag ratio

of zero corresponds to drag-only control with no lift while a ballistic coefficient ratio of one corresponds to lift-only control with a ballistic coefficient of 450 kg/m^2. The lowest ballistic coefficients and vertical lift-to-drag ratios, the unshaded region in Fig 33, are not feasible. While increasing both the vertical lift-to-drag ratio and ballistic coefficient ratio decreases the minimum PMF, increasing the ballistic coefficient ratio has a larger effect than increasing the lift-to-drag ratio. For a lift-only control system, adding a drag modulation event with even a low ballistic coefficient ratio could significantly reduce the propellant for this high-ballistic coefficient vehicle. For example, the PMF of a lift-only control system with a lift-to-drag ratio of 0.18 would see a 41% reduction in PMF from 0.1943 to 0.1144 by adding drag modulation with a ballistic coefficient ratio of 2.

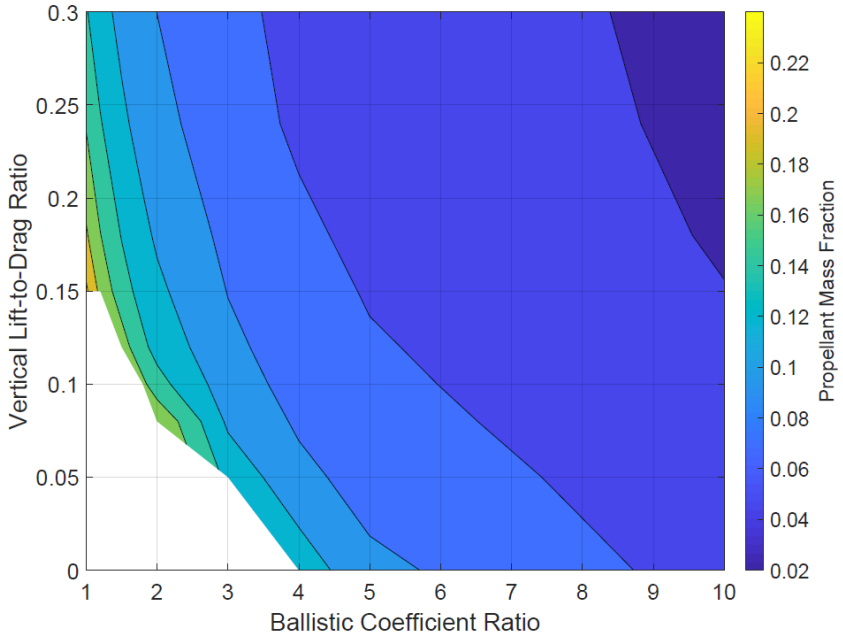

Fig 33. Lift-and-Drag Control, Minimum PMF for Various Vertical Lift-to-drag Ratios and Ballistic Coefficient Ratios for β = 450 kg/m^2 and V_0 = 5845 m/s

The ballistic coefficient of the vehicle was varied from the nominal, 450 kg/m^2, to a lower value of 300 kg/m^2 and larger value of 600 kg/m^2. The resulting trade in control options of the different ballistic coefficient vehicles for a lift-and-drag control system are shown in Fig 34 and Fig 35, respectively. For the lower ballistic coefficient shown in Fig 34, more of the lower ballistic coefficient ratios and vertical lift-to-drag ratios are feasible while less of these are feasible for the higher ballistic coefficient vehicle. For example a drag-only system with a ballistic coefficient ratio of at least 3 can meet landing constraints at the nominal entry conditions with a ballistic coefficient of 300 kg/m^2 but a vehicle with a ballistic coefficient of 450 kg/m^2 requires a ballistic coefficient ratio of at least 4. A drag-only vehicle with a ballistic coefficient of 600 kg/m^2 requires a larger ballistic coefficient ratio of at least 5.

The minimum PMF can still be significantly lowered by adding drag control to a lift-only vehicle with both the lower and higher ballistic coefficient. For a lift-only vehicle with a vertical lift-to-drag ratio of 0.18 and a ballistic coefficient of 300 kg/m^2, adding drag control with a ballistic coefficient ratio of 2 would reduce the PMF from 0.15 to 0.09164, a 39% reduction. For a similar vehicle with a ballistic coefficient of 600 kg/m^2, adding the drag control would reduce the PMF by 42% from 0.2349 to 0.1352. While the magnitude of the PMF is lower for the lower ballistic vehicle, the reduction in PMF by adding drag control to lift-only vehicles is fairly constant, only increasing by 3% as the ballistic increased from 300 kg/m^2 to 600 kg/m^2.

The entry velocity of the vehicle was varied from the nominal, 5,845 m/s, to a lower value of 5,000 m/s and larger value of 7,000 m/. The resulting trade in control options for the entry velocities for a lift-and-drag control system are shown in Fig 36 and Fig 37, respectively. As the entry velocity is lowered, the required vertical lift-to-drag ratio for a lift-only system is significantly larger. A lift-only system needs a vertical lift-to-drag ratio of at least 0.24 to meet

landing constraints at an entry velocity of 5000 m/s while an entry velocity of 5845 m/s only needs a vertical lift-to-drag ratio of at least 0.15. Furthermore, an entry at 7000 m/s needs a vertical lift-to-drag ratio of at least 0.12. All entry velocities for a drag-only vehicle need a ballistic coefficient ratio of at least 4.

The PMF of a lift-only system can again be drastically reduced by adding drag control with a ballistic coefficient ratio of 2. With an entry velocity of 5000 m/s, the PMF of a lift-only system with a vertical lift-to-drag ratio of 0.24 can be reduced from 0.1716 to 0.1039, a 39% reduction, while an entry at 7000 m/s would yield a reduction of 61% from 0.1578 to 0.09822. Adding drag control to a lift-only system would reduce the required PMF significantly more at larger entry velocities.

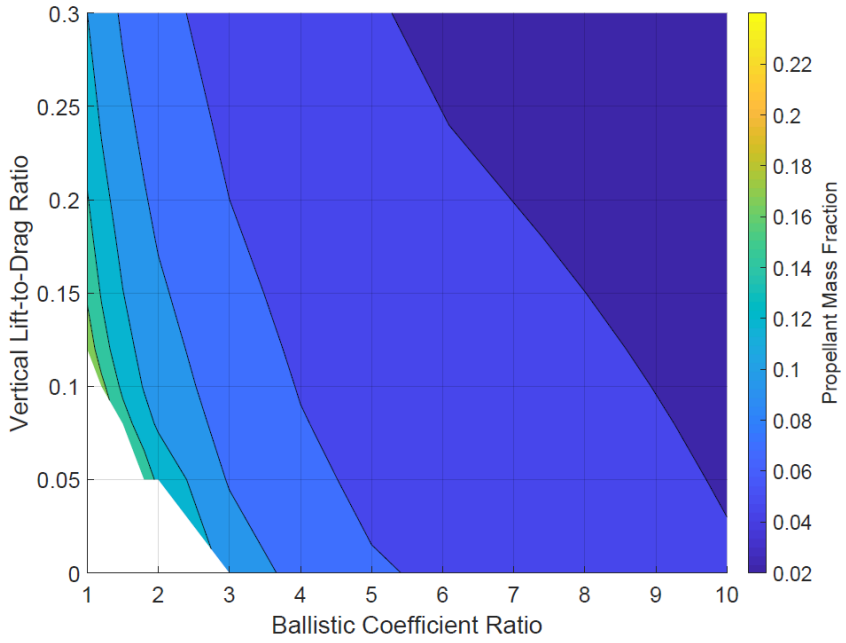

Fig 34. Lift-and-Drag Control, Minimum PMF for Various Vertical Lift-to-drag Ratios and Ballistic Coefficient Ratios for $\beta = 300$ kg/m^2 and $V_0 = 5845$ m/s

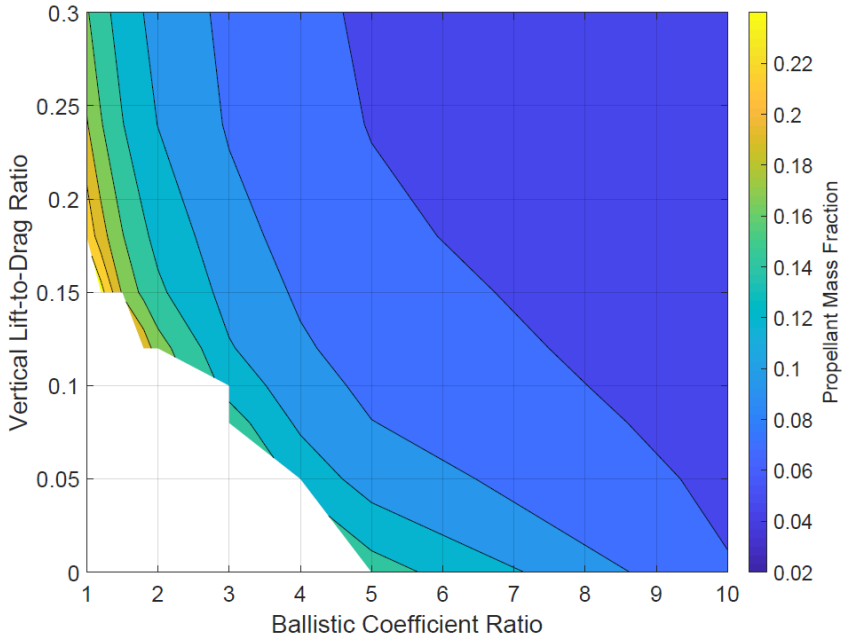

Fig 35. Lift-and-Drag Control, Minimum PMF for Various Vertical Lift-to-drag Ratios and Ballistic Coefficient Ratios for β = 600 kg/m^2 and V_0 = 5845 m/s

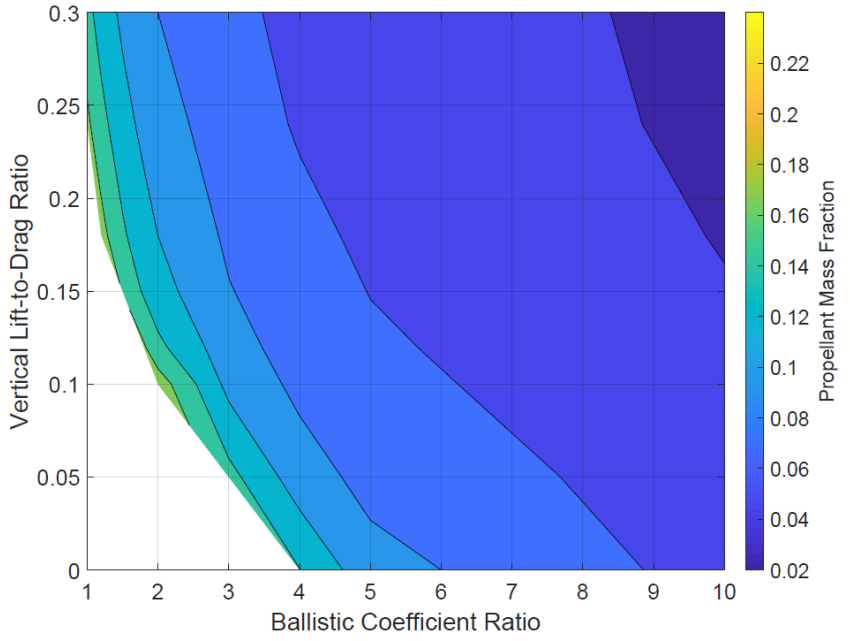

Fig 36. Lift-and-Drag Control, Minimum PMF for Various Vertical Lift-to-drag Ratios and Ballistic Coefficient Ratios for β = 450 kg/m^2 and V_0 = 5000 m/s

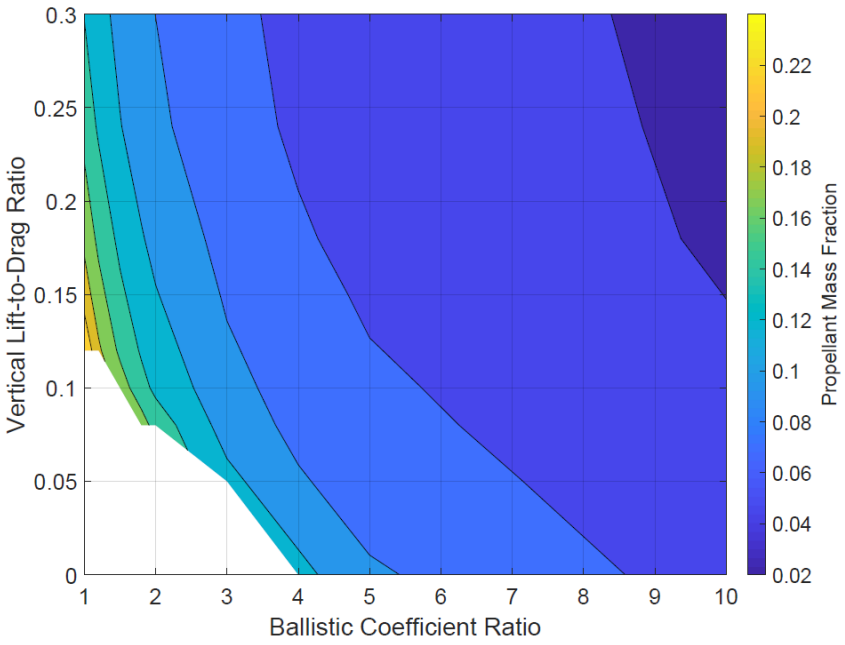

Fig 37. Lift-and-Drag Control, Minimum PMF for Various Vertical Lift-to-drag Ratios and Ballistic Coefficient Ratios for β = 450 kg/m^2 and V_0 = 7000 m/s

4.5 Reachable and Controllable TDI States

While there is a single TDI state that would yield the minimum PMF, it may not always be possible or best to target this state. Targeting a PMF-optimal TDI state may not be robust and can be susceptible to dispersions [18]. Therefore, reachable TDI states that nearly minimize the PMF for a set of TDI velocities and flight-path angles were examined.

Given the two-phase optimization problem to minimize PMF, there will be a reachable set of TDI states that are possible to achieve for the hypersonic control and a set of TDI states that are controllable for the propulsive descent phase. Starting at an initial entry state as specified in Table 2, the reachable set of TDI states is a three-dimensional volume, since the state vector is three-dimensional. However, given that the vehicle must land safely, there will also be a set of TDI states for which the propulsive descent phase is controllable; there is a set of TDI states for which thrust

control can be applied to achieve a feasible landing. Also, the constraint of a PMF optimal trajectory places a constraint on this controllable set. The altitude must be minimum, reducing the controllable set of TDI states from a volume to a surface. The problem then becomes to link the set of TDI states reachable by the hypersonic control and the reduced set of TDI states controllable for the propulsive descent phase.

4.5.1 Reachable Sets of TDI States

A cross-section of the reachable and controllable sets at a TDI velocity of 500 m/s, assuming only a maximum of two switches for lift-only control with a 0.24 lift-to-drag ratio, is shown in Fig 38. The entire reachable and controllable sets are defined by a volume and surface, respectively; however, only a cross-section at a TDI velocity of 500 m/s is shown. The reachable set is defined by the black and green lines and red and cyan dots which are the terminal states of all possible hypersonic trajectories of one or two switch cases integrated at 1 Hz using a fourth-order Runge-Kutta method. The purple line indicates the cross section of the controllable set of TDI states as defined in the previous section for a thrust to weight ratio of 4 and TDI velocity of 500 m/s. The intersection of this purple line and the reachable states is the feasible set that the hypersonic control method can target to meet landing constraints with the SRP system and minimize PMF. This intersection is also what Lorenz and Putnam [17] defined as the reachable TDI space. Control profiles at the boundaries, the shallowest and steepest TDI flight-path angles, match those seen by Lorenz and Putnam; a two-switch control profile at the steepest TDI flight-path angles is PMF optimal while a one-switch control profile is optimal at shallow flight-path angles.

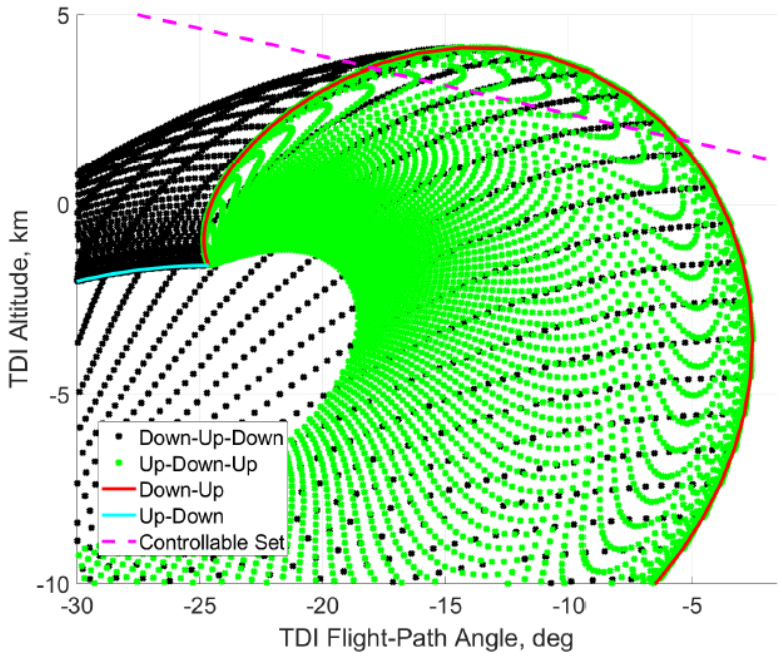

Fig 38 Cross-section of lift-only control reachable set at a L/D of 0.24 and controllable set of the SRP phase with a T/W of 4. The TDI velocity is 500 m/s.

A cross-section of the reachable and controllable sets at a TDI velocity of 500 m/s for a drag-only control system with a lift-to-drag ratio of 0.24 and ballistic coefficient of 2 is shown in Fig 40. Only a maximum of two switches was assumed; however, previous sections have shown that entry conditions that are not at risk of skipping-out do not have a large loft, so a one or two-switch control profile is optimal for both objective functions examined. While the drag-only control reachable set contains higher TDI altitude states than the lift-only control, the TDI flight-path angles of the drag-only control tend to be steeper. The drag-only control reachable set is also symmetric across the terminal states of the two possible one and two-switch control profiles.

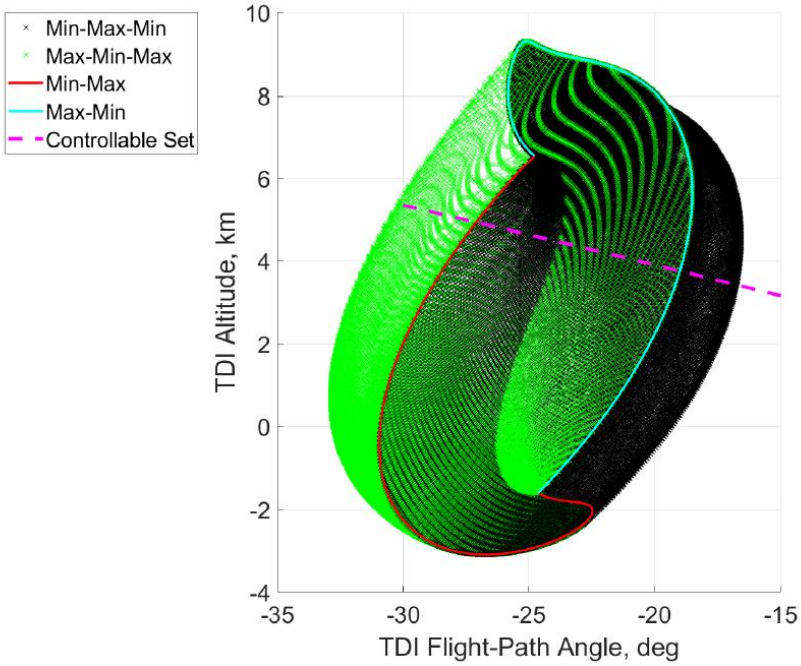

Fig 39. Cross-section of drag-only control reachable set at a L/D of 0.24, β_{ratio} of 2, and controllable set of the SRP phase with a T/W of 4. The TDI velocity is 500 m/s.

A cross-section of the reachable and controllable sets at a TDI velocity of 500 m/s for a low-lift, drag-only control system with a lift-to-drag ratio of 0.1 and ballistic coefficient of 2 is shown in Fig 40. Again, only a maximum of two switches was assumed. The reduction in lift of the drag-only control leads to shallower TDI flight-path angles and lower TDI altitudes being reachable. The reachable set of the low-lift, drag-only control is also bounded by the one-switch control terminal states shown in red and cyan lines with the terminal states of the two-switch control profiles encased within the terminal states of the one-switch control profiles.

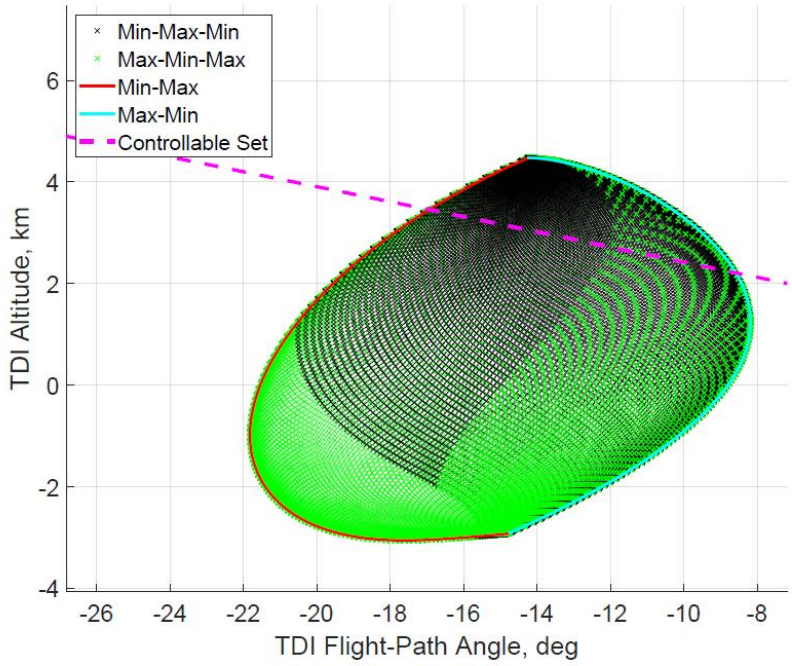

Fig 40. Cross-section of drag-only control reachable set at a L/D of 0.1, β_{ratio} of 2, and controllable set of the SRP phase with a T/W of 4. The TDI velocity is 500 m/s.

4.5.2 Lift-only Control Feasible TDI States

The intersection of the reachable and controllable sets of TDI states for a lift-only control system with various vertical lift-to-drag ratios is shown in Fig 41 as a projection of the reachable set onto the controllable set surface. As shown in Fig 33, a lift-only control system cannot meet landing constraints below a vertical lift-to-drag ratio of 0.15. At a vertical lift-to-drag ratio of 0.15, the feasible space, shown as the interior of the blue boundary in Fig 41, is narrow and disappears with lower vertical lift-to-drag ratios. For vertical lift-to-drag ratios less than 0.15, the intersection reachable set and controllable set cross-sections, shown in Fig 38, shrinks and vanishes; the projection onto the controllable set surface does not exist. As the vertical lift-to-drag ratio increases, the feasible space gradually expands uniformly, and a lower PMF is possible.

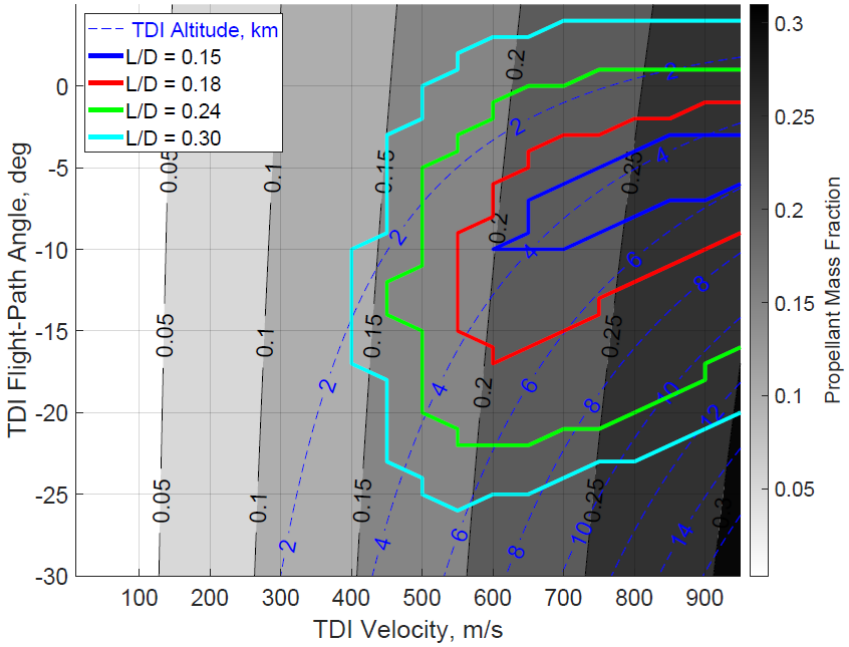

Fig 41. Lift-only Control, Reachable States over Various Lift-to-Drag Ratios

4.5.3 Drag Control Feasible TDI States

The intersection of the reachable and controllable sets of TDI states for a drag-only control system with no lift and various ballistic coefficient ratios is shown in Fig 42 as a projection of the reachable set onto the surface of the controllable set. As the ballistic coefficient ratio decreases, the feasible space narrows and shrinks. As the ballistic coefficient ratio increases, the feasible space gradually expands, and a lower PMF is possible.

Lift was added to the drag-only control but not used in the control. The lift was assumed always lift-up with a lift-to-drag ratio of 0.1. The intersection of the reachable and controllable sets is for the drag-only control with this low-lift shown in Fig 43. The addition of lift allows for an expansion of the feasible space at lower ballistic coefficient ratios with a feasible space at a ballistic coefficient as low as 1.5 becoming visible. Again increasing the ballistic coefficient ratio

gradually expands the feasible space with a lower PMF possible. Lift also expands the reachable TDI flight-path angles to shallower angles.

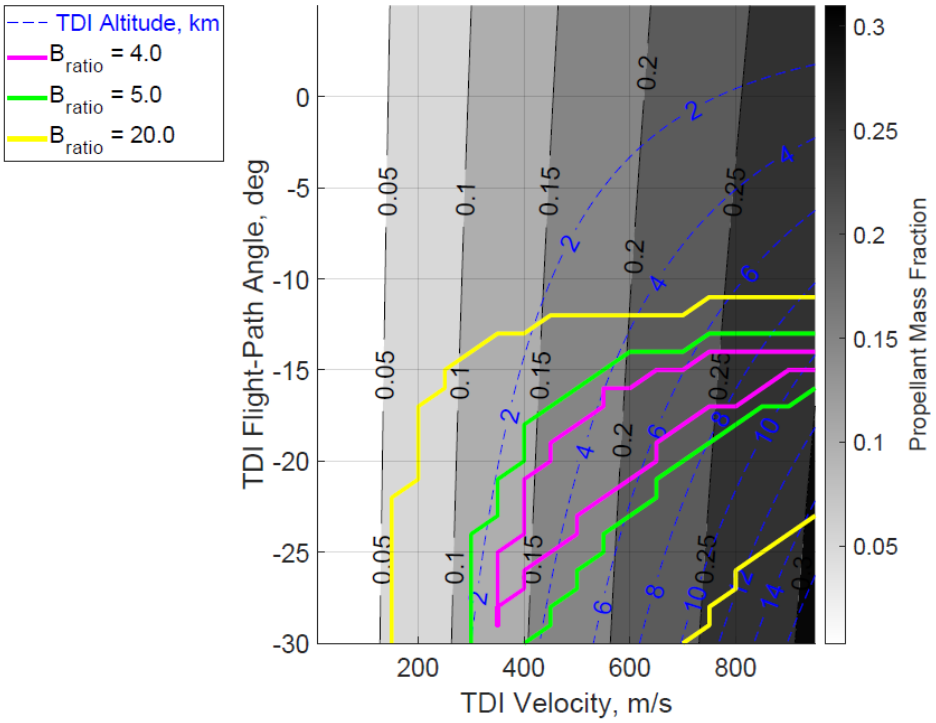

Fig 42. Drag-only Control, Reachable States over Various Ballistic Coefficient Ratios for No Lift, L/D = 0

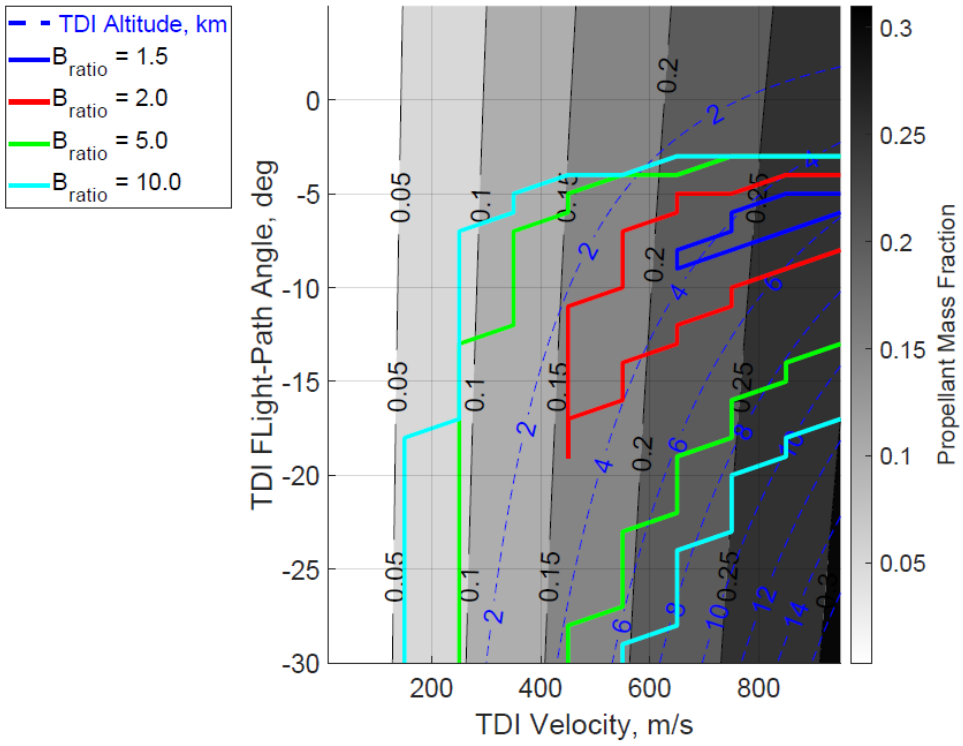

Fig 43. Drag-only Control, Reachable States over Various Ballistic Coefficient Ratios for L/D = 0.1

4.5.4 Lift-and-Drag Control Feasible TDI States

The intersection of the reachable and controllable sets of TDI states for a lift-and-drag control system with a lift-to-drag ratio of 0.1 and various ballistic coefficient ratios is shown in Fig 44. At a lift-to-drag ratio of 0.1, lift-only control is not feasible; there are no reachable and controllable TDI states that intersect for the test vehicle configuration. For this case, the addition of drag control with a ballistic coefficient ratio of 1.5 becomes mission enabling. As the ballistic coefficient ratio increases, the feasible space gradually expands and a lower PMF is possible.

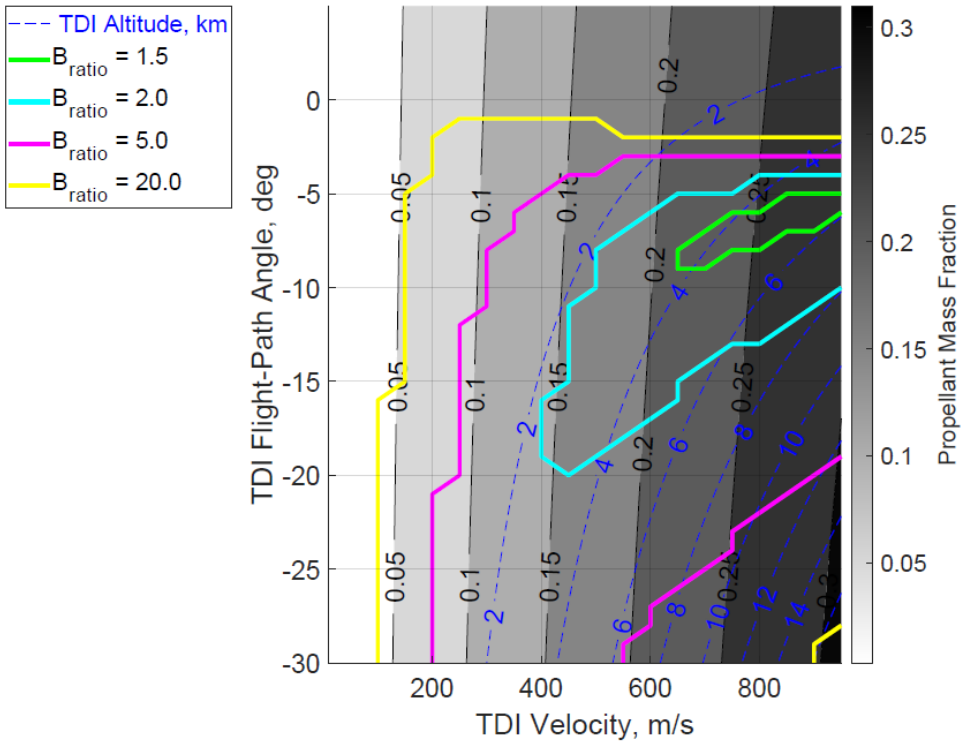

Fig 44. Lift-and-Drag Control with L/D of 0.1, Reachable States over Various Ballistic Coefficient Ratios

When lift is increased to a vertical lift-to-drag ratio of 0.24 for the lift-and-drag system, lift-only control is possible as shown by the blue boundary of a ballistic coefficient ratio of 1 in Fig 45. With the larger lift, the feasible space is larger than the low-lift case at a vertical lift-to-drag ratio of 0.1 and again gradually expands as drag control is added with increasing ballistic coefficient ratios. At large ballistic coefficients, 10 and 20, the feasible space incorporates most of the design space.

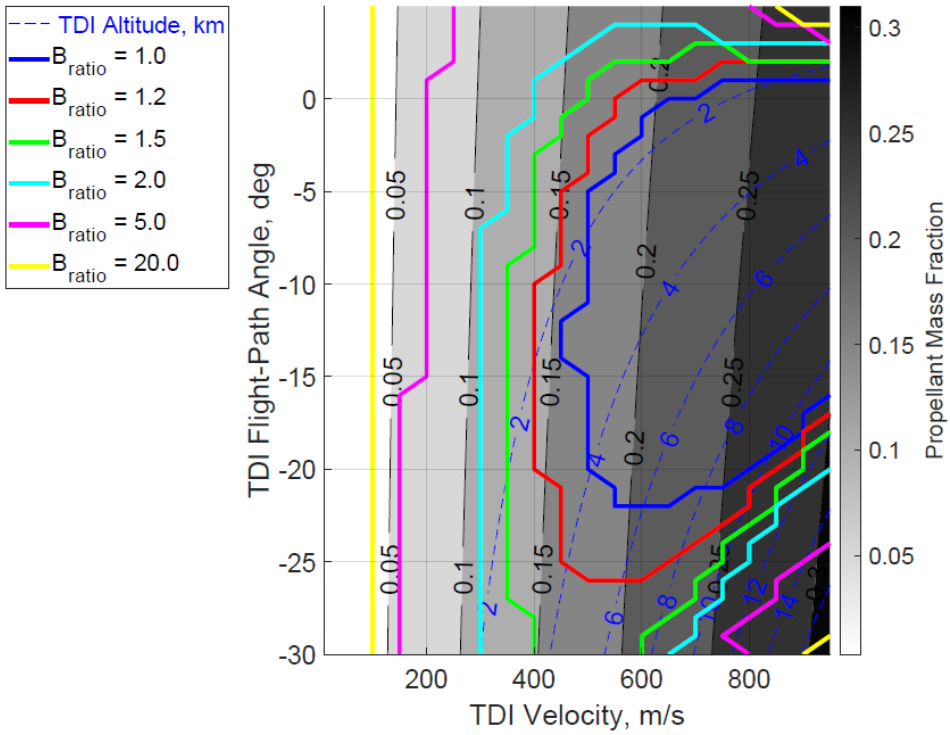

Fig 45. Lift-and-Drag Control with L/D of 0.24, Reachable States over Various Ballistic Coefficient Ratios

CHAPTER 5: CONCLUSIONS

Significant technology development will be required for future, larger mass missions at Mars. Current Viking-era parachute technology will not be feasible to use in the near future as payload mass and ballistic coefficient increases. SRP has been identified as a key technology to enable these larger ballistic coefficient missions; however, most previous work on targeting optimal states to begin the descent phase have focused on using bank angle control and maximizing TDI altitude. While the maximization of the TDI altitude is an appropriate parameter for parachute deployment systems, it is not propellant-optimal for SRP systems. Furthermore, developments in decelerator technology make another hypersonic flight control option, drag modulation, more viable. Other control options using control of both lift and drag include direct force control or a simple combination of lift and drag control.

The ability of lift-only control, drag-only, and lift-and-drag hypersonic trajectory control schemes to maximize TDI altitude or minimize PMF over a range of entry conditions were compared at Mars using optimal control techniques. For TDI altitude maximization, both lift-only and drag-only control achieved a highest maximum TDI altitude at moderate entry flight-path angles, approximately -20º for lift-only and -19º for drag-only control, and the largest entry velocity examined, 7 km/s. Both control options exhibited multiple optimal control profiles, depending primarily on entry flight-path angle. The lift-only system had two optimal control profiles, lift-up at the steepest entry flight-path angles or a one-switch, entering lift-down to lift-up, at shallow entry flight-path angles, above -18º at a 5 km/s entry velocity to -21º at a 7 km/s entry velocity. The drag-only system optimal control profile ranged from no-switch, always minimum ballistic coefficient, at the steepest entry flight-path angles to four-switches at the shallowest entry flight-path angles, avoiding a long loft period. All optimal control profiles were

bang-bang. The highest maximum TDI altitude entry condition occurred at a one-switch control profile for both systems. The optimal lift-only control enters lift-down with a switch to lift-up towards the end of its trajectory while the optimal drag-only control enters at a maximum ballistic coefficient and switches to a minimum ballistic coefficient at the end of its trajectory. Similar trends in optimal control profiles for the PMF minimization were seen for both systems although the PMF-optimal entry state occurred at the largest entry velocity, 7 km/s, and steepest entry flight-path angle, -25º, with a reduced minimum PMF with larger entry velocity and steeper entry flight-path angle.

Drag-only control was found to be superior for both cost functions when the entry vehicle entered the Martian atmosphere at a steep initial flight-path angle. For TDI altitude maximization, drag-only control was superior between entry flight-path angles of approximately -14.5º and -22º with some variation across various entry velocities. Above a -14.5º entry flight-path angle the lift-only control method yielded a larger TDI altitude. Below a -22º entry flight-path angle, the two methods were identical, always lift-up, minimum ballistic coefficient. For the PMF minimization, lift-only control was superior above 17.5º at a 5 km/s entry velocity to -21.5º at a 7 km/s entry velocity.

The lift-and-drag control system showed similar behavior to a combination of the lift-only and drag-only systems across both cost functions. The main difference in optimal control profiles of the lift-and-drag control was the loss of the four and three-switch optimal drag control profiles seen in the drag-only control. This loss is thought to be the result of the lift-down command available to decrease lofting in the lift-and-drag control system. All optimal control was found to be bang-bang, despite a non-linearity of the control in the Hamiltonian. The lift-and-drag control always led to a larger maximum TDI altitude or lower minimum PMF compared to the lift-only

and drag-only control systems at shallow entry flight path angles. For TDI altitude maximization, lift-and-drag control was superior to the lift-only control above -20º entry flight-path angle at 5 km/s entry velocity and -21.6º at an entry velocity of -21.6º. Lift-and-drag control was superior to the drag-only control above -15.8º entry flight-path angle at 5 km/s entry velocity and -21.6º at an entry velocity of -18.9º. For PMF minimization, the lift-and-drag control was generally 1% lower PMF than the lift-only control for almost all entry conditions examined with the exception of the steepest, slowest entry conditions. The lift-to-drag control had as much as a 5% lower PMF than the drag-control at shallow flight-path angles, above -20.5º at an entry velocity of 5 km/s and -23.5 at an entry velocity of 7 km/s. At steeper entry flight-path angles, the lift-and-drag optimal control profiles were always lift-up and always minimum ballistic coefficient, resembling those of the lift-only and drag-only optimal control.

The trade between the vertical lift-to-drag ratio and ballistic coefficient ratio for a lift-and-drag control system was examined, finding a generally greater decrease in PMF by adding drag modulation to a lift-only control system than adding lift modulation to a drag-only system with ballistic coefficients of 450 kg/m^2. A reduction in PMF of 40% was found in a lift-only control system with a vertical lift-to-drag ratio of 0.18 by adding drag modulation with a ballistic coefficient of 2. The reduction in PMF was similar for ballistic coefficients of 300 kg/m^2 and 600 kg/m^2; however, increasing the initial velocity to 7 km/s increased the reduction in PMF to 61% by adding drag control. Generally, adding drag control to high ballistic coefficient, lift-only vehicles reduces the PMF with a greater reduction achieved at higher entry velocities. The minimum ballistic coefficient ratio needed for a drag-only system was found to increase with an increasing ballistic coefficient but remain constant at 4 for various entry velocities from 5 km/s to

7 km/s. The minimum vertical lift-to-drag ratio needed for a lift-only system to be feasible was found to increase with a larger ballistic coefficient and lower entry velocity.

The intersection between the reachable and controllable sets of TDI states for all methods was explored. For a maximum of two-switches, the drag-only control was found to have a reachable set defined by the two possible one-switch, bang-bang control profiles while lift-only control did not show this behavior. Increasing the ballistic coefficient ratio was found to gradually increase the size of the feasible set, the intersection of the reachable and controllable sets; increasing the hypersonic control authority increases the reachability.

Future work should examine the cost of the optimal trajectories shown in this work. The optimal drag control trajectories require an increase in drag area at some point in the hypersonic flight and are likely to lead to impractical decelerations or heat rates. An alternative formulation of using some of the additional control authority given by including both lift and drag control to mitigate these parameters may be necessary.

REFERENCES

[1] Braun, R. D., and Manning, R. M., "Mars Exploration Entry, Descent, and Landing Challenges," Journal of Spacecraft and Rockets, Vol. 44, No. 2, 2007, pp. 310–323. Doi: 10.2514/25116

[2] Braun, R. D., and Manning, R. M., "Mars Exploration Entry, Descent, and Landing Challenges," IEEE Aerospace Conference, IEEE Paper 0076, Piscataway, NJ, 2006. doi:10.1109/AERO.2006.1655790

[3] Edquist, K.T.,Korzun, A.M.,Dyakonov, A. A., Studak, J.W.,Kipp, D.M.,and Dupzyk, I.C., "Development of Supersonic Retropropulsion for Future Mars Entry, Descent, and Landing Systems," Journal Spacecraft and Rockets, Vol. 51, No. 3, 2014, pp. 650–663. doi:10.2514/1.A32715

[4] Korzun, A. M., and Braun, R. D., "Performance Characterization of Supersonic Retropropulsion for High-Mass Mars Entry Systems," Journal of Spacecraft and Rockets, Vol. 47, No. 5, 2010, pp. 836–848. doi:10.2514/1.49803

[5] Korzun, A. M., and Braun, R. D., "Conceptual Modeling of Supersonic Retropropulsion Flow Interactions and Relationships to System Performance," Journal of Spacecraft and Rockets, Vol. 50, No. 6, 2013, pp. 1121–1133. doi:10.2514/1.A32464

[6] Skeen, M. A., and Starkey, R. P., "Conceptual Modeling of Drag-Augmented Supersonic Retropropulsion for Mars Entry, Descent, and Landing," Journal of Spacecraft and Rockets, Vol. 51, No. 6, 2014, pp. 1924–1942. doi:10.2514/1.A32920

[7] Mandalia, A. B., and Braun, R. D., "Supersonic Retropropulsion Thrust Vectoring for Mars Precision Landing," Journal of Spacecraft and Rockets, Vol. 52, No. 3, 2015, pp. 827–835. doi:10.2514/1.A33119

[8] Pritchard, E. B., and Harrison, E. F., "Lifting Entry (L/D <= 0.2) for Unmanned Viking Class Mars Landers," NASA TN D-5828, Washington, D.C., 1970. Doi: 10.2514/6.1971.22

[9] García-Llama, E., "Apollo-Derived Terminal Control for Bank-Modulated Mars Entries with Altitude Maximization," AIAA Guidance, Navigation and Control Conference and Exhibit, AIAA Paper 2008-6819, 2008. doi:10.2514/6.2008-6819

[10] Lafleur, J. M., and Cerimele, C. J., "Mars Entry Bank Profile Design for Terminal State Optimization," Journal of Spacecraft and Rockets, Vol. 48, No. 6, 2011, pp. 1012–1024. doi:10.2514/1.51944

[11] Lafleur, J. M., and Cerimele, C. J., "Angle of Attack Modulation for Mars Entry Terminal State Optimization," AIAA Atmospheric Flight Mechanics Conference, AIAA Paper 2009-5611, 2009. doi:10.2514/6.2009-5611

[12] Benito, J., and Mease, K. D., "Reachable and Controllable Sets for Planetary Entry and Landing," Journal of Guidance, Control, and Dynamics, Vol. 33, No. 3, 2010, pp. 641–654. doi:10.2514/1.47577

[13] Grant, M. J., and Mendeck, G. F., "Mars Science Laboratory Entry Optimization Using Particle Swarm Methodology," AIAA Atmospheric Flight Mechanics Conference and Exhibit, AIAA Paper 2007-6393, 2007. doi:10.2514/6.2007-6393

[14] Lu, P., "Entry Trajectory Optimization with Analytical Feedback Bank Angle Law," AIAA Guidance, Navigation and Control Conference and Exhibit, AIAA Paper 2008-7268, 2008. doi:10.2514/6.2008-7268

[15] Jacob, G. L., Neeler, G., and Ramanan, R. V., "Mars Entry Mission Bank Profile Optimization," Journal of Guidance, Control, and Dynamics, Vol. 37, No. 4, 2014, pp. 1305–1316. doi:10.2514/1.G000089

[16] Anderson, T. R., Putnam, Z. R., and Braun, R. D., "Strategies for Landing Large Ballistic Coefficient Vehicles on Mars," AIAA Atmospheric Flight Mechanics Conference, AIAA Paper 2016–0021, 2016. doi:10.2514/6.2016-0021

[17] Lorenz, C. G., Putnam, Z. R., "Optimal Hypersonic Trajectories for High Ballistic Coefficient Vehicles at Mars," Journal of Spacecraft and Rockets, 2019, pp 0-12. doi: 10.2514/1.A34262

[18] Lu, P., "Propellant-Optimal Powered Descent Guidance," Journal of Guidance, Control, and Dynamics, Vol. 41, No. 4, 2018, pp. 813-826. doi: 10.2514/1.G003243

[19] Lu. P., "Augmented Apollo Powered Descent Guidance," Journal of Guidance, Control, and Dynamics, Vol. 42, No. 3, 2019, pp. 447-457. doi: 10.2514/1.G004048

[20] Mendeck, G. F., and McGrew, L. C., "Entry Guidance Design and Postflight Performance for 2011 Mars Science Laboratory Mission," Journal of Spacecraft and Rockets, Vol. 51, No. 4, 2014, pp. 1094–1105. doi:10.2514/1.A32737

[21] Graves, C. A., and Harpold, J. C. "Apollo Experience Report – Mission Planning for Apollo Entry," NASA TN D-6725, Washington, D.C. 1972

[22] Putnam, Z. R., and Braun, R. D., "Precision Landing at Mars Using Discrete-Event Drag Modulation," Journal of Spacecraft and Rockets, Vol. 51, No. 1, 2014, pp. 128-138. doi: 10.2514/1.A32633

[23] Putnam, Z. R., and Braun, R. D., "Drag-Modulation Flight-Control System Options for Planetary Aerocapture," Journal of Spacecraft and Rockets, Vol. 51, No. 1, 2014, pp. 139-150. doi: 10.2514/1.A32589

[24] Cianciolo, A. M. D., Davis, J. L.,Komar, D. R., Munk, M. M., Samareh, J. A., Powell, R. W., Shidner, J. D., Stanley, D. O., Wilhite, A. W., Kinney, D., McGuire, M. K., Arnold, J. O., Howard, A. R., Sostaric, R. R., Studak, J., Zumwalt, C. H., Llama, E. G., Casoliva, J., Ivanov, M. C., Clark, I. G., and Sengupta, A., "Entry, Descent and Landing Systems Analysis Study," NASA Langley Research Center TM-2010-216720,Hampton, VA, 2010.

[25] Cianciolo, A. M. D., Davis, J. L., Engelund,W. C.,Komar, D. R., Queen, E. M., Samareh, J. A.,Way, D.W., Zang, T. A., Murch, J. G., Krizan, S. A., Olds, A. D., Powell, R.W., Shidner, J. D., Kinney, D., McGuire, M. K., Arnold, J. O., Covington, M. A., Sostaric, R. R., Zumwalt, C. H., and Llama, E. G., "Entry, Descent and Landing Systems Analysis Study," NASA Langley Research Center TM-2011-217055, Hampton, VA, 2011.

[26] Korzun, A. M., Murphy, K. J., and Edquist, K. T., "Supersonic Aerodynaminc Characteristics of Blunt Body Trim Tab Configurations," *AIAA Applied Aerodynamics Conference,* AIAA Paper 2013-2809, 2013. doi: 10.2514/6.2013-2809

[27] Horvath, T. J., O'Connell, T. F., Cheatwood,, F. M., Prabhu, R. K., and Alter, S. J., "Experimental Hypersonic Aerodynamic Characteristics of Mars Surveyor 2001 Precision Lander with Flap," Journal of Spacecraft and Rockets, Vol. 43, No.2, 2006, pp. 270-281. doi: 10.2514/1.19651

[28] Byrne, R. H., Robinett, R. D., and Sturgis, B. R., "Moving mass trim control system design," *AIAA Guidance, Navigation, and Control Conference,* AIAA Paper 96-3826, 1996, doi: 10.2514/6.1996-3826
[29] Atkins, B. M., and Queen, E. M., "Internal Moving Mass Actuator Control for Mars Entry Guidance," Journal of Spacecraft and Rockets, Vol. 52, No. 5, 2015, pp. 1294-1310. doi: 10.2514/1.A32970
[30] Venkatapathy, E., Arnold, J., Fernandez, I., Hamm, K. R., Kinney, D., Laub, B., Makino, A., McGuire, M. K., Peterson, K, Prabhu, D., Empey, D., Dupzyk, I., Huynh, L., Hajela, P., Gage, P., Howard, A., Andrews, D., "Adaptive Deployable Entry and Placement Technology (ADEPT): A Feasibility Study for Human Missions to Mars," *AIAA Aerodynamic Decelerator Systems Technology Conference and Seminar,* AIAA Paper 20100-2608, 2011. doi: 10.2514/6.2011-2608
[31] Wooster, P. D., Braun, R. D., Ahn, J., and Putnam, Z. R., "Mission Design Options for Human Mars Missions," International Journal of Mars Science and Exploration, Vol. 3, Aug. 2007, pp. 12–28. doi:10.1555/mars.2007.0002
[32] Patterson, M. A., and Rao, A. R., GPOPS-II–Next-Generation Optimal Control Software, Software Package, Ver. 2.1.3, RP Optimization Research, LLC, Gainesville, FL, 2013.
[33] Christian, J. A., Wells, G., Lafleur, J., Verges, A., and Braun, R. D., "Extension of Traditional Entry, Descent, and Landing Technologies for Human Mars Exploration," Journal of Spacecraft and Rockets, Vol. 45, No. 1, 2008, pp. 130–141. doi:10.2514/1.31929
[34] McInnes, C. R., "Gravity Turn Descent with Quadratic Air Drag," Journal of Guidance, Control, and Dynamics, Vol. 20, No. 2, 1997, pp. 393–394.doi:10.2514/2.4052
[35] Steinfeldt, B. A., "Guidance, Navigation, and Control System Performance Trades for Mars Pinpoint Landing," Journal of Spacecraft and Rockets, Vol. 47, No. 1, 2010, pp. 188–198. doi:10.2514/1.45779